

# 1 On the formation of highly oxidized pollutants by autoxidation 2 of terpenes under low temperature combustion conditions: the 3 case of limonene and $\alpha$ -pinene.

4 Roland Benoit<sup>1</sup>, Nesrine Belhadj<sup>1,2</sup>, Zahraa Dbouk<sup>1,2</sup>, Maxence Lailliau<sup>1,2</sup>, and Philippe Dagaut<sup>1</sup>

5 <sup>1</sup>CNRS-INSIS, ICARE, Orléans, France, roland.benoit@cnrs-orleans.fr, nesrine.belhadj@cnrs-orleans.fr,  
6 zahraa.dbouk@cnrs-orleans.fr, maxence.lailliau@cnrs-orleans.fr, dagaut@cnrs-orleans.fr

7 <sup>2</sup>Université d'Orléans, Orléans, France

8 **Correspondence:** Roland Benoit ([roland.benoit@cnrs-orleans.fr](mailto:roland.benoit@cnrs-orleans.fr))

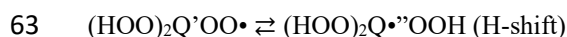
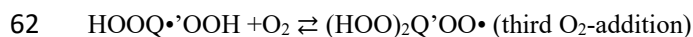
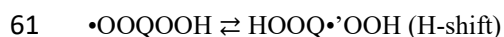
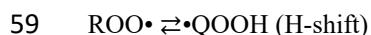
## 10 **Abstract.**

11 The oxidation of monoterpenes under atmospheric conditions has been the subject of numerous studies. They were  
12 motivated by the formation of oxidized organic molecules (OOM) which, due to their low vapor pressure,  
13 contribute to the formation of secondary organic aerosols (SOA). Among the different reaction mechanisms  
14 proposed for the formation of these oxidized chemical compounds, it appears that the autoxidation mechanism,  
15 involving successive events of O<sub>2</sub> addition and H-migration, common to both low-temperature combustion and  
16 atmospheric conditions, is leading to the formation of highly oxidized products (HOPs). However, cool flame  
17 oxidation (~500-800 K) of terpenes has not received much attention even if it can contribute to atmospheric  
18 pollution through biomass burning and wildfires. Under such conditions, terpenes can be oxidized via autoxidation.  
19 In the present work, we performed oxidation experiments with limonene-oxygen-nitrogen and  $\alpha$ -pinene-oxygen-  
20 nitrogen mixtures in a jet-stirred reactor (JSR) at 590 K, a residence time of 2 s, and atmospheric pressure.  
21 Oxidation products were analyzed by liquid chromatography, flow injection, and soft ionization-high resolution  
22 mass spectrometry. H/D exchange and 2,4-dinitrophenyl hydrazine derivatization were used to assess the presence  
23 of OOH and C=O groups in oxidation products, respectively. We probed the effects of the type of ionization used  
24 in mass spectrometry analyses on the detection of oxidation products. Heated electrospray ionization (HESI) and  
25 atmospheric pressure chemical ionization (APCI), in positive and negative modes were used. We built an  
26 experimental database consisting of literature data for atmospheric oxidation and presently obtained combustion  
27 data for the oxidation of the two selected terpenes. This work showed a surprisingly similar set of oxidation  
28 products chemical formulas, including oligomers, formed under the two rather different conditions, i.e., cool flame  
29 and simulated atmospheric oxidation. Data analysis (in HESI mode) indicated that a subset of chemical formulas  
30 is common to all experiments, independently of experimental conditions. Finally, this study indicates that more  
31 than 45% of the detected chemical formulas in this full dataset can be ascribed to an autoxidation reaction.

### 33 1 Introduction

34 Terpenes are emitted into the troposphere by vegetation (Seinfeld and Pandis, 2006). They can be used as drop in  
 35 fuels (Harvey et al., 2010;Mewalal et al., 2017;Harvey et al., 2015) which could increase emissions via fuel  
 36 evaporation and unburnt fuel release. Biomass burning and wildfires can also release terpenes and their products  
 37 of oxidation into the troposphere (Gilman et al., 2015;Hatch et al., 2019;Schneider et al., 2022). Wildfires  
 38 temperature ranges from 573 to 1373 K (Wotton et al., 2012), which covers both the cool flame (~500-800 K) and  
 39 intermediate to high temperature combustion regimes. Products of biomass burning have been characterized earlier  
 40 (Smith et al., 2009). Using van Krevelen diagrams, the authors reported H/C versus O/C in the ranges 0.5 to 3 and  
 41 0 to 1, respectively. Whereas a large fraction of these products can derive from cellulose, hemicellulose, and lignin  
 42 oxidation, their formation via terpenes oxidation cannot be ruled out. In a more recent study (Gilman et al., 2015),  
 43 it was reported that biomass burning emissions were dominated by oxidized organic compounds (57 to 68% of  
 44 total mass emissions). Wildfires are getting more and more frequent and their intensity increases(Burke et al.,  
 45 2021). In large wildfires, there are many updrafts which can transport a variety of materials ranging from gases to  
 46 particulates, and even bacteria (Kobziar et al., 2018). Furthermore, it was recently demonstrated that recent  
 47 wildfires in Australia produced smoke which could reach an altitude of 35 km (Khaykin et al., 2020). Such events  
 48 could contribute to ozone destruction (Bernath et al., 2022) but also to tropospheric pollution. But, field  
 49 measurements are not appropriate for comparison with the present data because a strict distinction on the origins  
 50 of the chemical compounds observed cannot be assessed. For example, literature works and reviews (Hu et al.,  
 51 2018;Popovicheva et al., 2019;Prichard et al., 2020) present field measurements from smoldering fires which were  
 52 not detailed enough to be used here.

53 Cool flame oxidation is dominated by autoxidation (Bailey and Norrish, 1952;Benson, 1981;Cox and Cole,  
 54 1985;Korcek et al., 1972) which involves peroxy radicals (ROO<sup>•</sup>). Autoxidation is based on an H-shift and oxygen  
 55 addition which starts with the initial production of ROO<sup>•</sup> radicals. This mechanism can repeat itself several times  
 56 and lead to recurrent oxygen additions to form highly oxidized products (Wang et al., 2017;Wang et al.,  
 57 2018;Belhadj et al., 2020;Belhadj et al., 2021a;Belhadj et al., 2021b):



65 There, the formation of highly oxidized products (HOPs) was mainly attributed to autoxidation reactions (Belhadj  
 66 et al., 2021c;Benoit et al., 2021).

67 In atmospheric chemistry, it is only relatively recently that this pathway has been considered (Vereecken et al.,  
 68 2007;Crouse et al., 2013;Jokinen et al., 2014a;Ehn et al., 2014;Berndt et al., 2015;Jokinen et al., 2015;Berndt et  
 69 al., 2016;Iyer et al., 2021). Also, it has been identified that highly oxygenated organic molecules (HOMs), a source  
 70 of secondary organic aerosols (SOA), can result from autoxidation processes (Ehn et al., 2014;Wang et al.,

71 2021;Tomaz et al., 2021;Bianchi et al., 2019). Modeling studies complemented by laboratory experiments showed  
72 that autoxidation mechanisms proceed simultaneously on different ROO<sup>•</sup> radicals leading to the production of a  
73 wide range of oxidized compounds in a few hundredths of a second (Jokinen et al., 2014a;Berndt et al.,  
74 2016;Bianchi et al., 2019;Iyer et al., 2021). Recent works have shown that, under certain atmospheric conditions,  
75 this autoxidation mechanism could be competitive with other reaction pathways involving ROO<sup>•</sup> radicals (Bianchi  
76 et al., 2019), e.g., the carbonyl channel ( $\text{ROO}^{\bullet} \rightarrow \text{R}_{\text{H}}\text{O} + \text{OH}$ ), the hydroperoxide channel ( $\text{ROO}^{\bullet} + \text{HOO}^{\bullet} \rightarrow$   
77  $\text{ROOH} + \text{O}_2$  and  $\text{RO}^{\bullet} + \text{OH} + \text{O}_2$ ), disproportionation reactions ( $\text{ROO}^{\bullet} + \text{R}'\text{OO}^{\bullet} \rightarrow \text{RO}^{\bullet} + \text{R}'\text{O}^{\bullet} + \text{O}_2$  and  $\text{R}_{\text{H}}\text{O} +$   
78  $\text{R}'\text{OH} + \text{O}_2$ ), accretion reactions ( $\text{ROO}^{\bullet} + \text{R}'\text{OO}^{\bullet} \rightarrow \text{ROOR}' + \text{O}_2$ ). Similarity, in terms of observed chemical  
79 formulas of products from cool flame oxidation of limonene and atmospheric oxidation of limonene, has been  
80 reported recently (Benoit et al., 2021). The same year, Wang et al. showed that the oxidation of alkanes follows  
81 this autoxidation mechanism under both atmospheric and combustion conditions (Wang et al., 2021). Also, that  
82 work confirmed that internal H-shifts in autoxidation can be promoted by the presence of functional groups, as  
83 predicted earlier (Otkjær et al., 2018) for ROO<sup>•</sup> radicals containing OOH, OH, OCH<sub>3</sub>, CH<sub>3</sub>, C=O, or C=C groups.  
84 Autoxidation will preferentially form chemical functions such as carbonyls, hydroperoxyl, or peroxy. This large  
85 diversity of chemical functions will promote the formation of isomers. Nevertheless, the common point to these  
86 chemical compounds is the sequential addition of O<sub>2</sub>. Therefore, in a database, potential candidate products of  
87 autoxidation are easily identified by this sequential addition.

88 To better understand the importance of these reaction pathways, the experimental conditions unique to these two  
89 chemistries must be considered. In laboratory studies conducted under simulated atmospheric conditions, oxidation  
90 occurs at near-ambient temperatures (250-300 K), at atmospheric pressure, in the presence of ozone and/or <sup>•</sup>OH  
91 radicals (Table S1), used to initiate oxidation with low initial terpene concentrations. In combustion, the <sup>•</sup>OH  
92 radical, temperature, and pressure are driving autoxidation. In addition to the increase in temperature, the initial  
93 concentrations of the reagents are generally higher compared to the atmospheric conditions, in order to initiate the  
94 oxidation with O<sub>2</sub>, which is much slower than that involving ozone or <sup>•</sup>OH. Rising temperature increases  
95 isomerization rates and favors autoxidation, at the expense of other possible reactions of ROO<sup>•</sup> radicals. Indeed, it  
96 has been reported earlier that a temperature rise from 250 to 273K does not affect the distribution of HOMs  
97 (Quéléver et al., 2019) whereas Tröstl et al. suggested that the distribution of HOMs is affected by temperature,  $\alpha$ -  
98 pinene or particle concentration (Tröstl et al., 2016). Similarly, the experiments of Huang et al. performed at  
99 different temperatures (223 K and 296 K) and precursor concentration ( $\alpha$ -pinene 0.714 and 2.2 ppm) suggested  
100 that the physicochemical properties, such as the composition of the oligomers (at the nanometer scale), can be  
101 affected by a variation of temperature (Huang et al., 2018). The broad range of chemical molecules formed and  
102 the impact of the experimental conditions on their character remains a subject for atmospheric chemistry as well  
103 as for combustion chemistry studies. Whatever the mechanism of aerosols formation, i.e., oligomerization,  
104 functionalization, or accretion, their composition will be linked to that of the initial radical pool (Camredon et al.,  
105 2010;Meusinger et al., 2017;Tomaz et al., 2021).

106 In low-temperature combustion, when the temperature is increased, fuel's autoxidation rate goes through a  
107 maximum between 500 and 670 K, depending on the nature of the fuel (Belhadj et al., 2020;Belhadj et al., 2021c).  
108 In low-temperature combustion chemistry as in atmospheric chemistry, the oxidation of a chemical compound  
109 leads to the formation of several thousands of chemical products which result from successive additions of oxygen,  
110 isomerization, accretion, fragmentation, and oligomerization (Benoit et al., 2021;Belhadj et al., 2021b). The

111 exhaustive analysis of chemical species remains, under the current instrumental limitations, impossible. Indeed,  
112 this would consist in analyzing several thousands of molecules using separative techniques such as ultra-high-  
113 pressure liquid chromatography (UHPLC) or ion mobility spectrometry (IMS) (Krechmer et al., 2016; Kristensen  
114 et al., 2016). Nevertheless, it is possible to classify these molecular species, considering only  $C_xH_yO_z$  compounds,  
115 according to criteria accessible via graphic tools representation such as van Krevelen diagrams, double bond  
116 equivalent number (DBE), and average carbon oxidation state (OSc) versus the number of carbon atoms  
117 (Kourtchev et al., 2015; Nozière et al., 2015). Such postprocessing of large datasets has the advantage of  
118 immediately highlighting classes of compounds or physicochemical properties such as the condensation of  
119 molecules (vapor pressure), the large variety of oxidized products ( $C_xH_yO_{1\text{ to }15}$  in the present experiments) and the  
120 formation of oligomers (Kroll et al., 2011; Xie et al., 2020).

121 In addition to the recent studies focusing on the first steps of autoxidation, a more global approach, based on the  
122 comparison of possible chemical transformations related to autoxidation in low temperature combustion and  
123 atmospheric chemistry, is needed for evaluating the importance of autoxidation under tropospheric and low-  
124 temperature combustion conditions. In order to study the effects of experimental conditions on the diversity of  
125 chemical molecules formed by autoxidation, we have selected  $\alpha$ -pinene and limonene, two isomeric terpenes  
126 among the most abundant in the troposphere (Zhang et al., 2018). Limonene has a single ring structure and two  
127 double bonds, one of which is exocyclic.  $\alpha$ -Pinene has a bicyclic structure and a single endo-cyclic double bond.  
128 These two isomers with their distinctive physicochemical characters are good candidates for studying autoxidation  
129 versus initial chemical structure and temperature. For  $\alpha$ -pinene, in addition to the reactivity of its endo-cyclic  
130 double bond, products of ring opening of the cyclobutyl group have been detected (Kurtén et al., 2015; Iyer et al.,  
131 2021), which could explain the diversity of observed oxidation products. This large pool of oxidation products is  
132 increased in the case of limonene by the presence of two double bonds (Hammes et al., 2019; Jokinen et al., 2015).

133 The present work extends that concerning the oxidation of limonene alone (Benoit et al., 2021). Compared to  
134 previous works, we have added the study of  $\alpha$ -pinene oxidation to that of limonene and investigated the impact of  
135 ionization modes on the number of molecules detected and their chemical nature (unsaturation, oxidation rate).  
136 The size of the experimental and bibliographic databases has been increased by more than 50%, in particular by  
137 adding data specific to autoxidation (Krechmer et al., 2016; Tomaz et al., 2021) and references on  $\alpha$ -pinene (Tab.  
138 2)). Here, we oxidized  $\alpha$ -pinene and limonene in a jet-stirred reactor at atmospheric pressure, excess of oxygen,  
139 and elevated temperature. We characterized the impact of using different ionization techniques (HESI and APCI)  
140 in positive and negative modes on the pool of detected chemical formulas. The particularities of each ionization  
141 mode were analyzed to identify the most suitable ionization technique for exploring the formation of autoxidation  
142 products under low temperature combustion. H/D exchange and 2,4-dinitrophenyl hydrazine derivatization were  
143 used to assess the presence of hydroperoxy and carbonyl groups, respectively. Chemical formulas detected here  
144 and in atmospheric chemistry studies were compiled and tentatively used to evaluate the importance of  
145 autoxidation routes under both conditions.

## 146 2 Experiments

### 147 2.1 Oxidation experiments

148 The present experiments were carried out in a fused silica jet-stirred reactor (JSR) setup presented earlier (Dagaut  
149 et al., 1986;Dagaut et al., 1988) and used in previous studies (Dagaut et al., 1987;Benoit et al., 2021;Belhadj et al.,  
150 2021c). We studied separately the oxidation of the two isomers,  $\alpha$ -pinene and limonene. As in earlier works (Benoit  
151 et al., 2021;Belhadj et al., 2021c),  $\alpha$ -pinene (+), 98% pure from Sigma Aldrich and limonene (R)-(+), >97% pure  
152 from Sigma Aldrich, were pumped by an HPLC pump (Shimadzu LC10 AD VP) with an online degasser  
153 (Shimadzu DGU-20 A3) and sent to a vaporizer assembly where it was diluted by a nitrogen flow. Each terpene  
154 isomer and oxygen, both diluted by  $N_2$ , were sent separately to a 42 mL JSR to avoid oxidation before reaching 4  
155 injectors (nozzles of 1 mm I.D.) providing stirring. The flow rates of nitrogen and oxygen were controlled by mass  
156 flow meters. Good thermal homogeneity along the vertical axis of the JSR was recorded (gradients of < 1 K/cm)  
157 by thermocouple measurements (0.1 mm Pt-Pt/Rh-10% wires located inside a thin-wall silica tube). In order to  
158 observe the oxidation of these isomers, which are not prone to strong self-ignition, the oxidation of 1% of these  
159 chemical compounds ( $C_{10}H_{16}$ ) under fuel-lean conditions (equivalence ratio 0.25, 56%  $O_2$ , 43%  $N_2$ ), was carried  
160 out at 590 K, atmospheric pressure, and a residence time of 2 s. Under these conditions, the oxidation of the two  
161 isomers is initiated by slow H-atom abstraction by molecular oxygen ( $RH + O_2 \rightarrow R' + HO_2^*$ ). The fuel radicals  
162  $R'$  react rapidly with  $O_2$  to form peroxy radicals which undergo further oxidation, characteristic of autoxidation.  
163 Nevertheless, this autoxidation mechanism, although predominant, is not exclusive and other oxidation  
164 mechanisms are possible (Belhadj et al., 2021b). In this case, there may be a random overlap of chemical formulas.  
165 The autoxidation criteria (two chemical formulas separated by two oxygen atoms) allows to limit or avoid these  
166 overlaps.

### 167 2.2 Chemical analyses

168 A 2 mm I.D. probe was used to collect samples. To measure low-temperature oxidation products ranging from  
169 early oxidation steps to highly oxidized products, the samples were bubbled into cooled acetonitrile (UHPLC grade  
170  $\geq 99.9$ ,  $T = 0^\circ C$ , 250 mL) for 90 min. The resulting solution was stored in a freezer at  $-15^\circ C$ . The stability of the  
171 products was verified. No detectable changes in the mass spectra were observed after more than one month which  
172 is consistent with previous findings (Belhadj et al., 2021c).

173 Analyses of samples collected in acetonitrile (ACN) were carried out via direct infusion (rate:  $3\mu L/min$  and  
174 recorded for 1 min for data averaging) in the ionization chamber of a high-resolution mass spectrometer (Thermo  
175 Scientific Orbitrap® Q-Exactive, mass resolution 140,000 and mass accuracy <0.5 ppm RMS). UHPLC conditions  
176 were: a Vanquish UHPLC Thermo Fisher Scientific with a C18 column (Phenomenex Luna,  $1.6\mu m$ ,  $110\text{ \AA}$ ,  
177  $100 \times 2.1\text{ mm}$ ). The column temperature was maintained at  $40^\circ C$ .  $3\mu ml$  of sample were eluted by mobile phase  
178 containing water-ACN mix (pure water, ACN HPLC grade) at a flow rate of  $250\mu L/min$  (gradient: 5% to 20%  
179 ACN -3 min, 20% to 65% ACN - 22 min, 65% to 75% ACN - 4 min, 75% to 90% ACN - 4 min, for a total of 33  
180 min).

181 Both heated electrospray ionization (HESI) and atmospheric chemical ionization (APCI) were used in positive and  
182 negative modes for the ionization of products. HESI settings were: spray voltage 3.8 kV, vaporizer temperature of

183 150°C, capillary temperature 200°C, sheath gas flow of 8 arbitrary units (a.u.), auxiliary gas flow of 1 a.u., sweep  
184 gas flow of 0 a.u.. In APCI, settings were: corona discharge current of 3µA, spray voltage 3.8 kV, vaporizer  
185 temperature of 150°C, capillary temperature of 200°C, sheath gas flow of 8 a.u., auxiliary gas flow of 1 a.u., sweep  
186 gas flow of 0 a.u.. In order to avoid transmission and detection effects of ions depending on their mass inside the  
187 C-Trap (Hecht et al., 2019), acquisitions with three mass ranges were performed (m/z 50-750; m/z 150-750; m/z  
188 300-750). The upper limit of m/z 750 was chosen because of the absence of a signal beyond this value. It was  
189 shown that no significant oxidation occurred in the HESI and APCI ion sources by injecting a limonene-ACN  
190 mixture (Fig. S1). The optimization of the Orbitrap ionization parameters in HESI and APCI did not show any  
191 clustering phenomenon for these two monoterpene isomers. The parameters evaluated were: injection source -  
192 capillary distance, vaporization and capillary temperatures, applied difference of potential, injected volume, flow  
193 rate of nitrogen in the ionization source. Positive and negative HESI mass calibrations were performed using  
194 Pierce<sup>TM</sup> calibration mixtures (Thermo Scientific). Chemical compounds with relative intensity less than 1 ppm to  
195 the highest MS signal in the mass spectrum were not considered. Nevertheless, it should be considered that some  
196 of the molecules presented in this study could result from our experimental conditions (continuous flow reactor,  
197 reagent concentration, temperature, reaction time) and to some extent from our acquisition conditions, different  
198 from those in the previous studies (Deng et al., 2021;Quéléver et al., 2019;Meusinger et al., 2017;Krechmer et al.,  
199 2016;Tomaz et al., 2021;Fang et al., 2017;Witkowski and Gierczak, 2017;Jokinen et al., 2015;Nørgaard et al.,  
200 2013;Bateman et al., 2009;Walser et al., 2008;Warscheid and Hoffmann, 2001;Hammes et al., 2019;Kundu et al.,  
201 2012). Operating with a continuous flow reactor, at elevated temperature, and high initial concentration of reagents  
202 allows the formation of combustion-relevant products, which does not exclude their possible formation under  
203 atmospheric conditions. To assess the formation of products containing OOH and C=O groups, as in previous  
204 works (Belhadj et al., 2021a;Belhadj et al., 2021b), H/D exchange with D<sub>2</sub>O and 2,4-dinitrophenyl hydrazine  
205 derivation were used, respectively.

### 206 3 Data Processing

207 High resolution mass spectrometry (HR-MS) generates large datasets which are difficult to fully analyze by  
208 sequential methods. When the study requires the processing of several thousands of molecules, the use of statistical  
209 tools and graphical representation means becomes necessary. In this study, we have chosen to use the van Krevelen  
210 diagram (Van Krevelen, 1950) by adding an additional dimension, the double bond equivalent (DBE). The DBE  
211 number represents the sum of unsaturation and rings present in a chemical compound (Melendez-Perez et al.,  
212 2016). The interest of this type of representation is to be able to identify more easily the clusters (increase of the  
213 DBE number at constant O/C and H/C ratios)

$$214 \quad \text{DBE} = 1 + C - H/2$$

215 This number is independent of the number of O-atoms, but changes with the number of hydrogen atoms. Decimal  
216 values of this number, which correspond to an odd number of hydrogen atoms, were not considered in this study.  
217 Then, the superpositions of points (and therefore of chemical formulas) in the O/C vs. H/C space are suppressed.  
218 The oxidation state of carbon (OSc) provides a measure of the degree of oxidation of chemical compounds (Kroll  
219 et al., 2011). This provides a framework for describing the chemistry of organic species. It is defined by the  
220 following equation:

221  $O_{Sc} \approx 2 O/C - H/C$

## 222 4 Results and discussion

223 We studied the oxidation of  $\alpha$ -pinene and limonene ( $C_{10}H_{16}$ ) at 590 K, under atmospheric pressure, with a residence  
 224 time of 2 s, and a fuel concentration of 1%. Under these conditions, the formation of peroxides by autoxidation at  
 225 low temperature should be efficient (Belhadj et al., 2021c), even though the conversion of the fuels remains  
 226 moderate.

### 227 4.1 Characterization of ionization sources

228 First, we have studied the impact of APCI and HESI sources, in positive and negative modes, on the chemical  
 229 formulas detected. The HESI and APCI sources in positive and negative mode were used and their operating  
 230 parameters were varied, i.e., temperature, gas flow and accelerating voltage (see Section 2). For each polarity, only  
 231 ions composed of carbon, hydrogen (even numbers) and oxygen were considered. Molecular duplicates inherent  
 232 to mass range overlaps were excluded. By following these rules, we obtained a different number of ions depending  
 233 on the ionization source and the polarity used. Table 1 shows the number of ions according to the experimental  
 234 conditions and the discrimination rules.

235 **Table 1.** Number of ions detected for each source in positive and negative modes (by protonation or  
 236 deprotonation, respectively)

Ionization source	$\alpha$ -Pinene		Limonene	
APCI	646 (R+H) <sup>+</sup>	503 (R-H) <sup>-</sup>	1321 (R+H) <sup>+</sup>	1346 (R-H) <sup>-</sup>
HESI	594 (R+H) <sup>+</sup>	693 (R-H) <sup>-</sup>	1017 (R+H) <sup>+</sup>	1864 (R-H) <sup>-</sup>

237  
 238 Each combination of ionization sources and polarity generated a set of chemical formulas. To make a meaningful  
 239 comparison between the positive and negative ions data, the chemical formulas used were the precursors of the  
 240 ions identified in the mass spectra. These sets have common data, but also specific chemical formulas. For a given  
 241 ionization source, ~ 50% of the chemical formulas are observed whatever the ionization polarity, i.e., using both  
 242 polarities one can capture between 30-50% more molecular species (since some of them are ionized under a single  
 243 mode (+ or -) depending on their chemical structure). Utilizing both ionization polarities is helpful for identifying  
 244 a larger quantity of species. The HESI source data were compared to the APCI data (Supplement, Tables S1 and  
 245 S2), showing an increased number (20 to 30%) of chemical formulas detected by HESI. This increase is  
 246 characterized by a better detection of negatively ionized species and those with a higher DBE. In order to evaluate  
 247 further the interest for using these ionization sources, we compiled these data in Venn diagrams and proposed a  
 248 visualization of these sets with a van Krevelen representation; we added the number of DBE in the third dimension  
 249 (Supplement, Tables S1 and S2).

250 In positive ionization mode, independently of the ionization source and in addition to the common molecular  
 251 formulas, we detected products with an O/C ratio < 0.2 whereas in the negative ionization mode, we detected  
 252 molecular formulas with an O/C ratio > 0.5. In addition to these observations, we noted that HESI is more

253 appropriate for studying products with a large number of unsaturation (DBE > 5), which is probably related to the  
254 increase in the number of hydroperoxide and carboxyl groups along with the fact that a heated ionization source  
255 favors vaporization of low volatility compounds. Finally, for an optimal detection of the oxidation products, it is  
256 necessary to consider the transmission limits of the C-Trap. Here, we could increase by more than 60% the number  
257 of molecular formulas detected using several mass ranges for data acquisition (section 2.2). The most appropriate  
258 ionization polarity to be used is tied to chemical functions present in products to be detected. We could increase  
259 by 30 to 100% the number of chemical formulas detected by using both positive and negative ionization modes.  
260 Using HESI is consistent with previous findings indicating ESI is well suited for the ionization of acidic, polar,  
261 and heteroatom-containing chemicals (Kekäläinen et al., 2013). To illustrate the present results, HESI (-)-MS  
262 spectra are provided in the Supplement (Fig. S2).

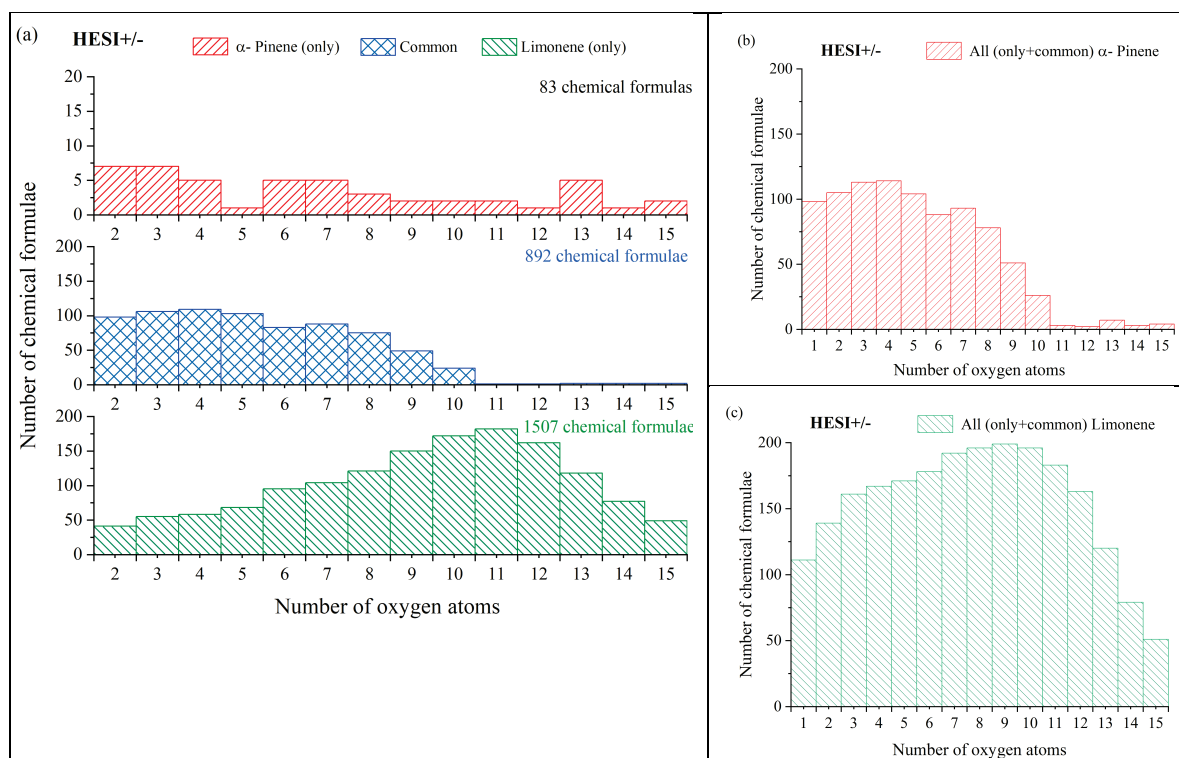
#### 263 4.2 Autoxidation products detected in a JSR

264 In order to compare the oxidation of  $\alpha$ -pinene and limonene, we compiled the positive and negative ionization data  
265 obtained with APCI (Table S1) and HESI (Table S2) ionization sources to obtain a more exhaustive database. For  
266 the APCI and HESI sources, we distinguished three datasets, two of which are specific to the oxidation of  $\alpha$ -pinene  
267 and limonene and one which is common to both isomers. In the following text, "only" will be used to describe the  
268 molecules specific to the oxidation of one of the isomeric terpenes. This common dataset represents more than  
269 77% of the chemical formulas identified in the  $\alpha$ -pinene oxidation samples detected with APCI. For limonene, for  
270 which the number of identified chemical formulas is greater, this common dataset represents over 93% of the  
271 chemical formulas detected after APCI ionization. In these two cases, the relatively low residence time (2 seconds)  
272 and the diversity of the chemical formulas obtained suggest that the oxidation of these two terpene isomers leads  
273 to ring opening, a phenomenon also observed in atmospheric chemistry (Berndt et al., 2016;Zhao et al., 2018;Iyer  
274 et al., 2021). Concerning the molecular formulas of products common to both isomers, Figure 1 shows that they  
275 are limited to compounds with 10 oxygen atoms or lower. This limit is linked to  $\alpha$ -pinene whose oxidation beyond  
276 10 oxygen atoms remains weak (less than 2% of the detected molecules for this terpene). In the case of limonene,  
277 the presence of an exocyclic double bond will increase, in a similar way to atmospheric chemistry (Kundu et al.,  
278 2012), the possibilities of oxidation and accretion. It remains however impossible, considering the size of the whole  
279 dataset and the diversity of the isomers, to formalize all the reaction mechanisms. Nevertheless, the formation of  
280 oxidized species can be described with the help of graphical tools. The number of oxygen atoms per molecule  
281 indicates that limonene oxidizes more than  $\alpha$ -pinene (Fig. 1a). In the case of limonene, with a HESI source,  
282 chemicals with an oxygen number of up to 15 were detected. Most of the chemical formulas recorded had 8-10 O-  
283 atoms (Fig. 1c), whereas for  $\alpha$ -pinene the products with >8 O-atoms were much less abundant (Fig. 1b). Moreover,  
284 for the products specific of limonene oxidation, this graph shows a distribution centered on 9 oxygen atoms with  
285 carbon skeletons probably resulting from accretion.

286

287





288  
 289 **Figure 1:** Distribution of  $\alpha$ -pinene and limonene autoxidation products as a function of their oxygen content  
 290 (ionization source: HESI, combined positive and negative modes data). (a)  $\alpha$ -pinene and limonene HESI(+/-),  
 291 (b)  $\alpha$ -pinene HESI(+/-), (c) limonene HESI(+/-)

292 To verify this accretion hypothesis, we can plot the OSc as a function of the number of carbon atoms or the O/C  
 293 ratio at fixed number of C-atoms (Fig. 2). Indeed, the presence of chemical compounds with 11 carbon atoms can  
 294 be explained by an accretion phenomenon (Wang et al., 2021), but the advantage of this OSc vs. nC space  
 295 representation (Kroll et al., 2011) is to allow studying this phenomenon on all the data. One can visualize the  
 296 evolution of the molecular oxidation for each carbon skeleton and the formation of oligomers. Species that are  
 297 unique to one of the isomers, or common to both are differentiated using different colors. In addition to the  
 298 autoxidation represented by the vertical axis for a given number of carbon atoms (Fig. 2a), we observe mechanisms  
 299 of fragmentation ( $C_{<10}$ ), accretion and oligomerization ( $C_{>10}$ ). These reaction mechanisms contribute to forming  
 300 chemical classes according to their number of carbon atoms. The increase in the number of oxygen atoms, but also  
 301 of carbon atoms will decrease products volatility. Following a classification proposed in the literature (Kroll et al.,  
 302 2011), we distinguished four sets of products: low volatile oxidized organic aerosols (LV-OOA), semi-volatile  
 303 oxidized organic aerosols (SV-OOA), biomass burning organic aerosols (BBOA) and water-soluble organic  
 304 carbons (WSOC). In the OSc versus carbon number plot (Fig 2a), the vertical lines (at constant carbon number)  
 305 are a first criterion for finding potential candidate products of autoxidation. Figure 2b shows, for a fixed number  
 306 of carbon and hydrogen atoms and a difference of two oxygen atoms, the potential products of autoxidation  
 307 connected by arrows whose color characterizes the oxygen parity. We can measure the extent of autoxidation for  
 308 each carbon backbone in the OSc vs. O/C space. Using these criteria, we found that 73% of all chemical formulas  
 309 are linked by a single difference of two oxygen atoms (which reflects an autoxidation mechanism). For the two  
 310 terpenes, for which the initial carbon number is equal to 10, one can observe (Fig. 2b) two autoxidation routes with  
 311 an even and odd number of oxygen atoms, respectively. This parity distinction is initially present for the two main

radicals, ROO $\cdot$  and RO $\cdot$  involved in autoxidation mechanisms. However, termination and propagation reactions will change the oxygen parity. Then, parity links between radicals and molecules are lost, which prevents interpretation of radical oxidation routes (Fig. 3). Figure 3 illustrates one of the reaction mechanisms (OH oxidation pathway) where oxygen parity changes through autoxidation. It should be noted that other reaction mechanisms can also change oxygen parity. In addition, the OH pathway in ozonolysis is not predominant. Figure 2 (b) illustrates the autoxidation routes between molecules resulting from a hydroperoxy radical reaction (arrows). In this case the oxygen parity is not modified and an OH radical is formed. HESI data showed an equivalent distribution of oxygen parities in molecular products (odd: 51%, even 49%) therefore confirming a lack of selectivity of the reaction mechanisms with respect to the oxygen parity of radicals.

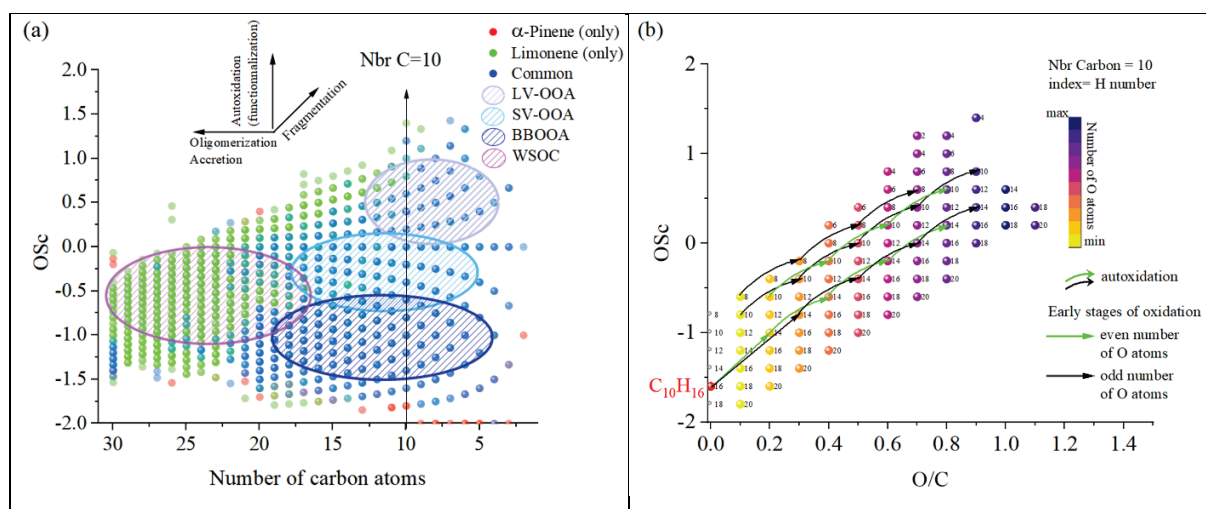
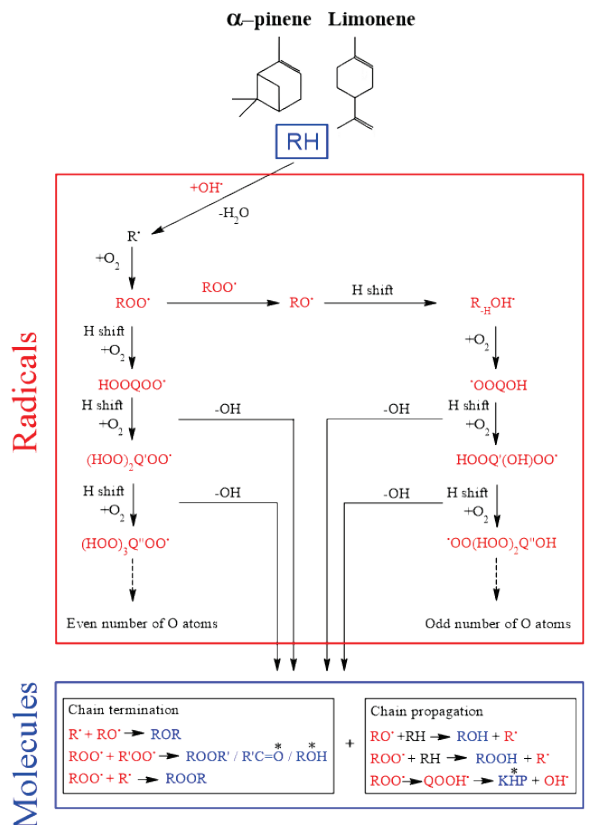


**Figure 2:** Overview of the distribution of limonene and  $\alpha$ -pinene oxidation products observed in a JSR: (a) OSc versus carbon number in detected chemical formulas from APCI and HESI data. (b) OSc versus O/C atomic ratio for a carbon number of 10; index of the products: number of hydrogen atoms. Arrows indicate autoxidation from a C<sub>10</sub>H<sub>16</sub> isomer, according to the oxygen parity in products



325  
 326 **Figure 3:** Accepted autoxidation reaction mechanisms in combustion (left) and in the atmosphere (left and right).  
 327 \* Indicates a change of oxygen atoms parity (Berndt et al., 2016).

328 **4.3 Combustion versus atmospheric oxidation**

329 *4.3.1 Global analysis*

330 We have explored potential chemical pathways related to autoxidation in the previous Section. For this purpose,  
 331 we have performed experiments under cool flame conditions (590 K). This autoxidation mechanism is also present  
 332 in atmospheric chemistry, but it is only recently that it has been found that this mechanism could be one of the  
 333 main formation pathways for SOA (Savee et al., 2015; Crounse et al., 2013; Jokinen et al., 2014a; Iyer et al., 2021).  
 334 Studies have described this mechanism in the case of atmospheric chemistry with the identification of radicals and  
 335 molecular species (Tomaz et al., 2021). However, previous studies on the propagation of this reaction mechanism  
 336 have mainly focused on the initial steps of autoxidation without screening all identified chemical formulas for  
 337 potential autoxidation products. It is therefore useful to assess the proportion of possible autoxidation products  
 338 among the total chemical species formed.

339 Here, we propose a new approach which consists in assessing a set of molecules mainly resulting from autoxidation  
 340 against different sets of experimental studies related to atmospheric chemistry. The objective is to evaluate  
 341 similarity of oxidation products formed under these conditions. For this purpose, we selected a HESI ionization  
 342 source, better suited for detecting higher polarity oxidized molecules, as well as higher molecular weight products  
 343 (detection of 96% of the total chemical formulas observed in autoxidation by APCI and HESI).

344 Among published atmospheric chemistry studies of terpenes oxidation, we have selected 15 studies presenting  
345 enough chemical products of oxidation, 4 for  $\alpha$ -pinene and 11 for limonene. The data were acquired using different  
346 experimental procedures (methods of oxidation, techniques of characterization). Table 2 summarizes all the  
347 experimental parameters related to the selected studies. From that Table, one can note that few studies involved  
348 chromatographic analyzes (Tomaz, 2021; Witkowski and Gierczak, 2017; Warscheid and Hoffmann, 2001). The  
349 data are from the articles or files provided in the Supplement Tables S1 and S2. In these studies, oxidation was  
350 performed only by ozonolysis with different experimental conditions that gather the main methods described in  
351 the literature: ozonolysis, dark ozonolysis, ozonolysis with OH scavenger, ozonolysis with or without seed  
352 particles. We considered that the ionisation mode used in mass spectrometry did not modify the nature of the  
353 chemical species but only the relative detection of ions, depending on the type of ionization used, and the  
354 sensitivity of the instruments (Riva et al., 2019). The combination of data obtained using (+/-) HESI gives a rather  
355 complete picture of the autoxidation products.

356 First, we compared the data from ozonolysis studies of each terpene and identified similarities through Venn  
357 diagrams. For studies with two ionization sources, duplicate chemical formulas were removed. We selected the  
358 four most representative studies by the number of the chemical formulas detected. Then, we compared the set of  
359 chemical formulas identified after ozonolysis to those produced in low-temperature combustion, the objective  
360 being (i) to highlight similarities in terms of products generated by the two oxidation modes and (ii) to identify  
361 chemicals resulting from autoxidation.

362

363

364 **Table 2.** Experimental settings of 15 oxidation studies of two terpenes under atmospheric conditions and cool  
 365 flames (LC stands for liquid chromatography).

Reference	Oxidation mode	Sampling	Experimental setup	Concentrations of reactants	Ionization /source	Instrument	Chemical formulas	LC
<b><math>\alpha</math>-Pinene</b>								
Y. Deng et al. (2021)	Dark ozonolysis seed particles OH scavenger	online	Teflon bag; 0.7m <sup>3</sup>	3.3±0.6 ncps ppbv <sup>-1</sup> $\alpha$ -Pinene	ESI	ToF-MS	351	No
Quéléver et al. (2019)	Ozonolysis	online	Teflon bag 5 m <sup>3</sup>	10 & 50 ppb $\alpha$ -Pinene	NO <sub>3</sub> <sup>-</sup> (CI)	CI-API-TOF	68	No
Meusinger et al. (2017)	Dark Ozonolysis OH scavenger no seed particles	offline	Teflon bag 4.5 m <sup>3</sup>	60 ppb $\alpha$ -Pinene	Proton transfer	PTR-MS-ToF	153	No
Krechmer et al. (2016)	Ozonolysis	offline	PAM Oxidation reactor	Field measurement	ESI (-) and NO <sub>3</sub> <sup>-</sup> (CI)	CI-IMS-ToF	43	No
This work	Cool-flame autoxidation	offline	Jet-stirred reactor 42 ml	1%, $\alpha$ -pinene No ozone	APCI(3kV) HESI (3kV)	Orbitrap® Q-Exactive	820 (APCI) 975 (HESI)	Yes
<b>Limonene</b>								
Krechmer et al. (2016)	Ozonolysis	offline	PAM Oxidation reactor	not specified	ESI (-) and NO <sub>3</sub> <sup>-</sup> (CI)	CI-IMS-ToF	63	No
Tomaz et al. (2021)	Ozonolysis	online	Flow tube reactor (18L)	45-227 ppb limonene	NO <sub>3</sub> <sup>-</sup> (CI) - Neg	Orbitrap® Q-Exactive	199	Yes
Fang et al. (2017)	OH-initiated photooxidation dark ozonolysis	online	Smog chamber	900–1500 ppb limonene	UV; 10 eV	Time-of-Flight (ToF)	17	No
Witkowski and Gierczak (2017)	Dark ozonolysis	offline	Flow reactor	2 ppm, limonene	ESI, 4.5 kV	Triple quadrupole	12	Yes
(Jokinen et al., 2015)	Ozonolysis	online	Flow glass tube	1–10000 x10 <sup>9</sup> molec.cm <sup>-3</sup> , limonene	NO <sub>3</sub> <sup>-</sup> (CI)	Time-of-Flight (ToF)	11	No
Nørgaard et al. (2013)	Ozone (plasma)	online	direct on the support	850 ppb ozone 15-150 ppb limonene	plasma	Quadrupole time-of-flight (QToF)	29	No
Bateman et al. (2009)	Dark and UV radiations ozonolysis	offline	Teflon FEP reaction chamber	1 ppm ozone 1 ppm limonene	modified ESI (+/-)	LTQ-Orbitrap Hybrid Mass (ESI)	924	No
Walser et al. (2008)	Dark ozonolysis	offline	Teflon FEP reaction chamber	1-10 ppm ozone 10 ppm limonene	ESI (+/-); 4.5 kV	LTQ-Orbitrap Hybrid Mass (ESI)	465	No
Warscheid & Hoffmann (2001)	Ozonolysis	online	Smog chamber	300-500 ppb limonene	APCI; 3kV	Quadrupole ion trap mass	21	Yes
Hammes et al., (2019)	Dark ozonolysis	online	Flow reactor	15, 40, 150 ppb limonene	<sup>210</sup> Po $\alpha$ acetate ions	HR-ToF-CIMS	20	No
Kundu et al. (2012)	Dark ozonolysis	offline	Teflon reaction chamber	250 ppb ozone 500 ppb limonene	ESI; 3.7 and 4 kV	LTQ FT Ultra, Thermo Sct (ESI)	1197	No
This work	Cool-flame autoxidation	offline	Jet-stirred reactor 42 ml	1%, limonene No ozone	APCI(3 $\mu$ A) HESI (3kV)	Orbitrap® Q-Exactive	1863(APCI) 2399(HESI)	Yes

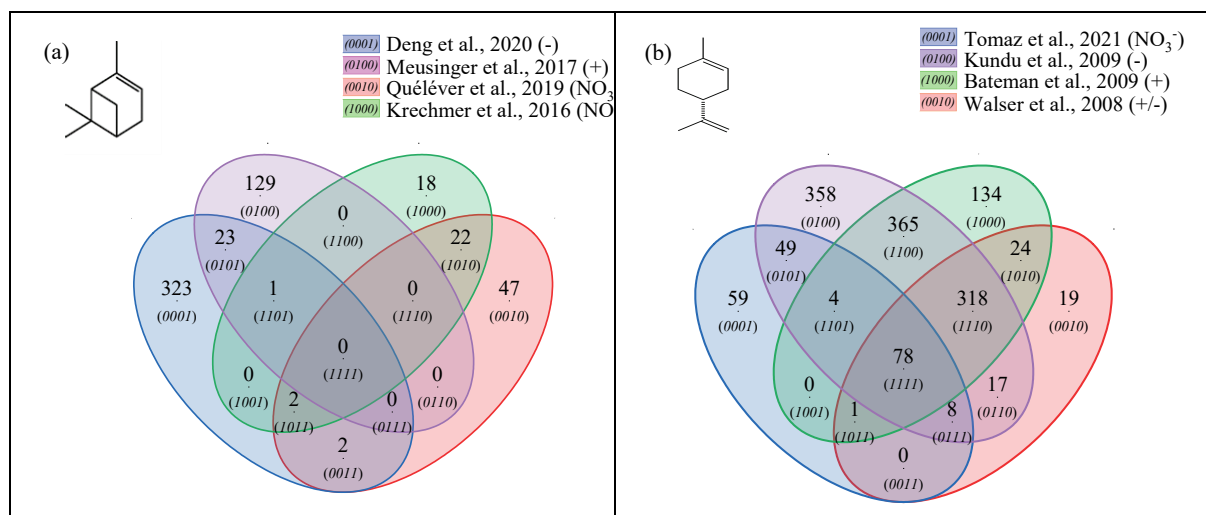
366

367 For  $\alpha$ -pinene oxidation, in the four selected studies 567 chemical formulas were detected, all polarities combined.

368 Only one study (Meusinger et al., 2017) was performed in positive ionization mode and none of the studies reported

369 data were obtained with two ionization modes (+/-). For the oxidation of limonene, the four selected studies  
 370 identified 1434 chemical formulas. Among these studies, the experiments by Walser et al. were performed with  
 371 both (+) and (-) ionisation modes. In contrast to the  $\alpha$ -pinene case, the selected studies for limonene were  
 372 performed with similar ionization sources, which probably contributed to increased data similarity (Walser et al.,  
 373 2008). In the case of limonene oxidation, for which accretion is more important than for  $\alpha$ -pinene, and for which  
 374 a greater number of chemical formulas were identified, the similarities are more important (Jokinen et al., 2014b).  
 375 These results are presented in Figure 4 where the ionization polarity used in each study is specified.

376



377 **Figure 4:** Venn diagrams for comparing the oxidation results from ozonolysis of (a)  $\alpha$ -pinene and (b) limonene  
 378 (see conditions in Table 1). Each digit indicates a study, the value of the digit characterizes the presence (value  
 379 1) or absence (0) common products detected in different studies, e.g., 23 chemical formulas (0101) (Fig. 4a) are  
 380 common to the studies of Deng et al; (0001) and Meusinger et al. (0100)

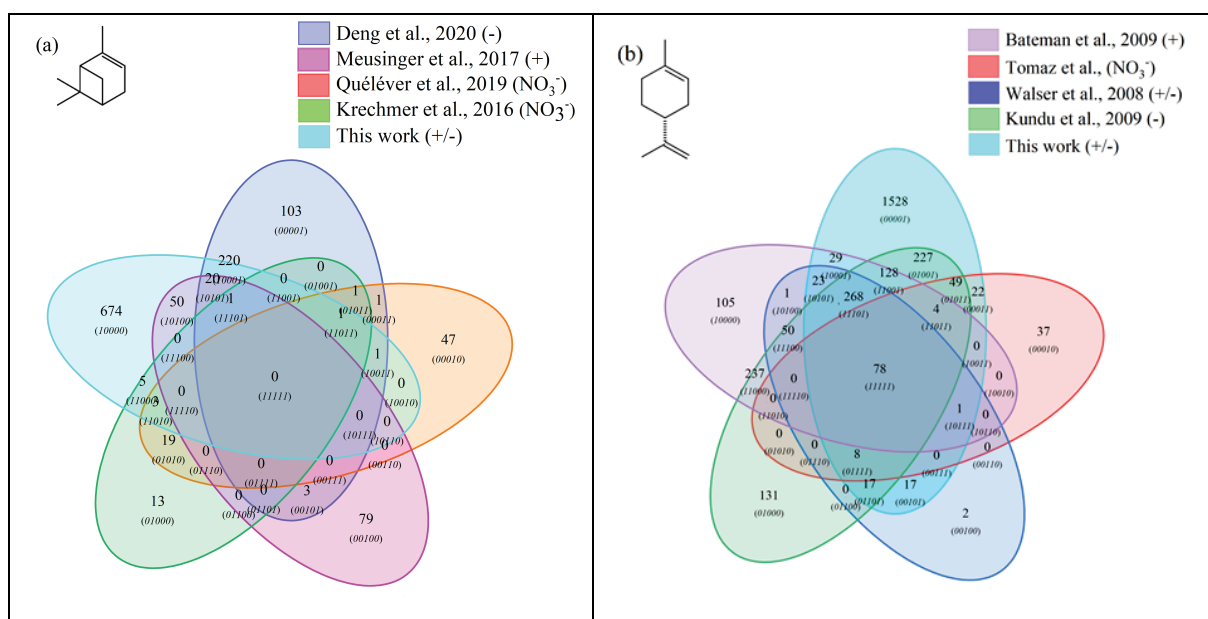
381 For  $\alpha$ -pinene, no chemical formula is common to all datasets. Different hypotheses can be offered to explain this  
 382 result. Among them, the number of chemical formulas identified per study remains limited (a few dozen to several  
 383 hundred) and these small datasets are sometimes restricted to specific mass ranges, e.g. C<sub>10</sub> to C<sub>20</sub> (Quéléver et al.,  
 384 2019). In the case of studies carried out with an NO<sub>3</sub><sup>-</sup> source, sensitive to HOMS, produced preferentially by  
 385 autoxidation, we note that nearly 50% of the chemical formulas (10/22; (1010)) are linked by a simple difference  
 386 of 2 oxygen atoms.

387 For limonene, 78 chemical formulas are common to the four studies selected here. In this data set, a large majority  
 388 of chemical formulas show a similar relationship to autoxidation, i.e., a simple difference of two oxygen atoms:  
 389 62% (Tomaz et al., 2021), 54% (Walser et al., 2008), 69% (Kundu et al., 2012), 66% (Bateman et al., 2009) and  
 390 72% (this study). This result seems to indicate that autoxidation dominates.

391 One can then ask if reaction mechanisms common to atmospheric and combustion chemistry can generate, despite  
 392 of radically different experimental conditions, a set of common chemical formulas and if in this common dataset,  
 393 a common link, characteristic of autoxidation, is observable? To address that question, we compared all the  
 394 previous results, for each of these terpenes to those obtained under the present combustion study. The comparisons  
 395 were made using our HESI data. One should remember that the oxidation conditions in the JSR were chosen in  
 396 order to maximize low-temperature autoxidation. Again, we used Venn diagrams to analyze these datasets

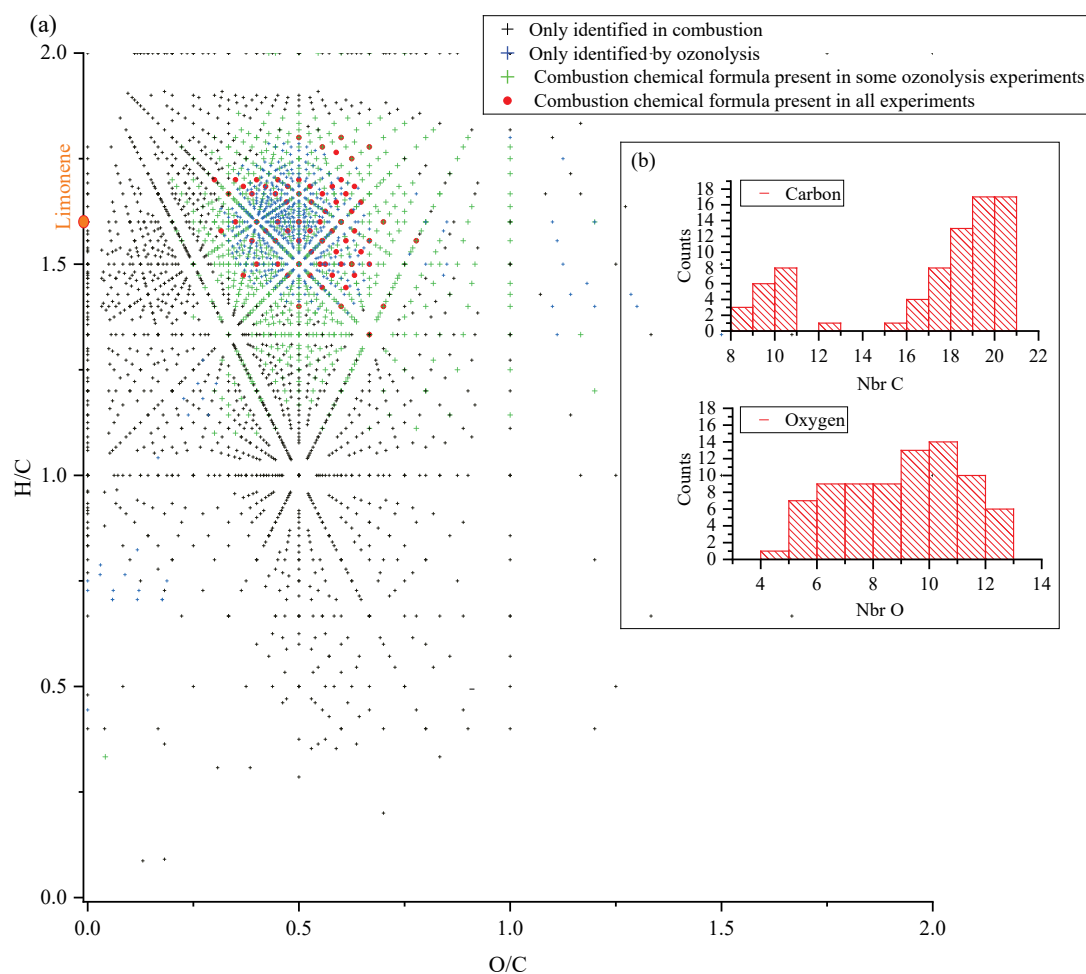
397 consisting of 1590 chemical formulas in the case of  $\alpha$ -pinene and 5184 chemical formulas in the case of limonene.  
 398 The results of these analyses are presented in Figure 5.

399 It turned out that for  $\alpha$ -pinene, 301 chemical formulas and for limonene 871 chemical formulas were common to  
 400 oxidation by ozonolysis (with or without scavenger) and combustion. This represents 31% of the chemical  
 401 formulas for the ozonolysis of  $\alpha$ -pinene and 36% for those of limonene ozonolysis. For  $\alpha$ -pinene, the similarities  
 402 compared to combustion are specific to each study: (Deng et al., 2021) 69% (243), (Meusinger et al., 2017) 46%,  
 403 (71) (Quéléver et al., 2019) 7% (5), (Krechmer et al., 2016) 23% (10). Chemical formulas common to all studies  
 404 were not identified. This lack of similarity may be due to a partial characterization of the chemical formulas, a  
 405 weaker oxidation of  $\alpha$ -pinene with an ionization mode less favorable to low molecular weights products.



406 **Figure 5:** Venn diagrams comparing the oxidation results from ozonolysis and combustion of (a)  $\alpha$ -pinene and  
 407 (b) limonene (see conditions in Table 1).

408 For limonene, the similarities with combustion are more important and less spread out. They represent for the  
 409 different studies: 65% (Kundu et al., 2012), 88% (Walser et al., 2008), 81% (Tomaz et al., 2021), and 57%  
 410 (Bateman et al., 2009). Moreover, there is a common dataset of 78 chemical formulas which can derive from  
 411 autoxidation mechanisms. Considering the very different experimental conditions, we must wonder about the  
 412 impact of the double bonds in this similarity. In the case of limonene, we think their presence will indeed promote  
 413 the formation of allylic radicals and then peroxide radicals (one of the motors of autoxidation). It is necessary to  
 414 specify again that different reaction mechanisms can cause the observed similarities. However, the preponderance  
 415 of autoxidation in so-called cool flame combustion is obvious, and in atmospheric chemistry, this reaction  
 416 mechanism is competitive or dominates (Crouse et al., 2013; Jokinen et al., 2014a). If we search for an  
 417 autoxidation link between these 78 chemical formulas, we observe that 45% of these chemical formulas meet this  
 418 condition: difference of two oxygen atoms between formulas, at constant number of carbon and hydrogen atoms.  
 419 More precisely, these molecules are centered in a van Krevelen diagram on the ratios  $O/C=0.6$  and  $H/C=1.6$ , in  
 420 the range  $0.29 < O/C < 0.77$  and  $1.33 < H/C < 1.8$ . All oxidized molecules associated with this dataset are presented  
 421 in Figure 6. The dispersion of the chemical formulas, far from being random, remains consistent with an  
 422 autoxidation mechanism where the numbers of carbon and hydrogen atoms are constant.

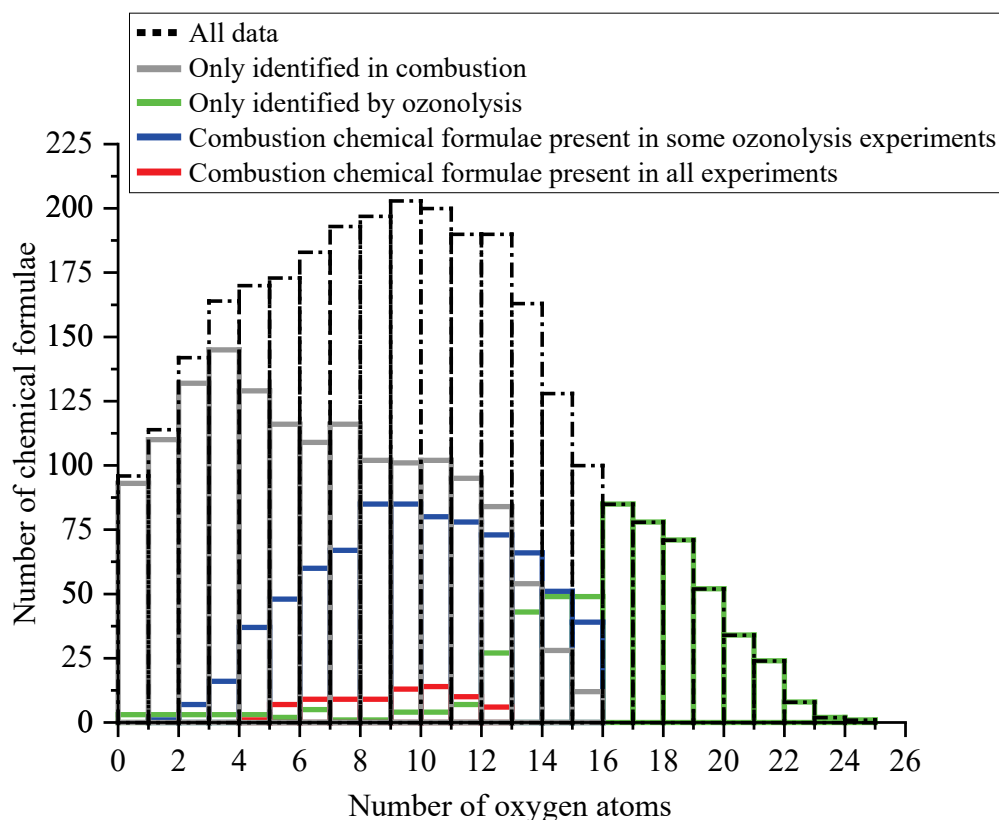


423  
 424 **Figure 6:** (a) Van Krevelen diagram showing specific and common chemical formulas detected after to  
 425 oxidation of limonene by ozonolysis and combustion, insert (b): distributions of the number of carbon and  
 426 oxygen atoms in the 78 chemical formulas common to all experiments.

427 A 3-D representation of all limonene oxidation data is given in Supplement (Fig. S3a) where DBE is used as third  
 428 dimension. From that figure, one can note that products with higher DBE (DBE>10) are preferably formed under  
 429 JSR conditions, i.e. at elevated temperature. A 2D representation (OSc vs DBE, Fig. S3b) completes this 3D view.  
 430 The corresponding chemical formulas with DBE > 10 could correspond to carbonyls and / or cyclic ethers ('QOOH  
 431 → carbonyl + alkene + OH and / or cyclic ether + OH'). Specificities and similarities of these two oxidation modes  
 432 (ozonolysis/combustion) were further investigated by plotting the distribution of the number of oxygen atoms in  
 433 detected chemical formulas (Fig. 7). Indeed, the distribution of the number of oxygen atoms allows, in addition to  
 434 the Van Krevelen diagram, to provide some additional details on these two modes of oxidation. In ozonolysis, we  
 435 observed the chemical formulas having the largest number of oxygen atoms. There, oxidation proceeds over a long  
 436 reaction time where the phenomenon of aging appears through accretion or oligomerization. In combustion, the  
 437 number of oxygen atoms remains limited to 18, with a lower number of detected chemical formulas compared to  
 438 the case of ozonolysis. However, it is in combustion that we observed the highest O/C ratios, indicating the  
 439 formation of the most oxidized products. This difference, however, does not affect the similarities between the  
 440 chemical formulas detected in the two modes of oxidation. Finally, the analysis of the parities in oxygen atoms,



441 very similar for the three datasets, confirms that the reaction mechanisms presented in Figure 3 do not allow a  
 442 simple link to be established between the oxygen parity of radicals and that of the detected molecular products.



443 **Figure 7:** Oxygen number distribution for all the molecules identified for the oxidation of limonene: only in  
 444 combustion, only in ozonolysis and common to both processes.  
 445

#### 446 4.3.2 Identification of common isomers.

447 We identified a set of chemical formulas common to both atmospheric and combustion chemistries and suggested  
 448 that this might result from an autoxidation mechanism. We identified several chemical formulas within this dataset  
 449 that differ by two oxygen atoms on the same skeleton. Focusing on the early stages of limonene oxidation, there  
 450 are several sequential two-oxygen additions to the chemical formulas  $C_{10}H_{16}O_2$  and  $C_{10}H_{16}O_3$  with the two oxygen  
 451 parities described in Figure 3. Tables 3 presents the identified chemical formulas with information on the Venn  
 452 index. The index for combustion is the rightmost (xxxx1).

453 Table 3. Sequential additions of two oxygens to the chemical formulas  $C_{10}H_{16}O_2$  and  $C_{10}H_{16}O_3$  present in the  
 454 common set of 78 chemical formulas.

First stages of oxidation	1st addition	2nd addition	3rd addition	4th addition	5th addition
$C_{10}H_{16}O_2$ (10101)	$C_{10}H_{16}O_4$ (11101)	$C_{10}H_{16}O_6$ (11111)	$C_{10}H_{16}O_8$ (01011)	$C_{10}H_{16}O_{10}$ (00011)	$C_{10}H_{16}O_{12}$ (00010)
$C_{10}H_{16}O_3$ (11101)	$C_{10}H_{16}O_5$ (11111)	$C_{10}H_{16}O_7$ (11111)	$C_{10}H_{16}O_9$ (01011)	$C_{10}H_{16}O_{11}$ (00010)	

455  
 456 This result of sequential additions of two oxygens is also observed for other chemical formulas of this common  
 457 dataset. Therefore, it questions the possibility that these two atmospheric and combustion chemistries develop  
 458 autoxidation mechanisms with common isomers.

459 In order to verify this possibility, considering the differences between limonene and  $\alpha$ -pinene, we analyzed by  
 460 UHPLC-HRMS the chemical compounds  $C_{10}H_{16}O_2$  for limonene and  $C_{10}H_{16}O_3$  for  $\alpha$ -pinene in the samples from  
 461 the combustion experiments. For limonene and  $\alpha$ -pinene, considering the availability of standards from suppliers,  
 462 we selected limonoaldehyde and pinonic acid, respectively. These two isomers of  $C_{10}H_{16}O_2$  and  $C_{10}H_{16}O_3$  are  
 463 among the most frequently reported products in atmospheric chemistry studies (Table 4). Our study shows same  
 464 retention times for these standards and isomers detected in combustion samples (Fig S4). This result is more  
 465 obvious for limonoaldehyde (11.5 min) than for pinonic acid (3.9 min). In addition, we detected the presence of -  
 466 OH or -OOH groups by H/D exchange with  $D_2O$  for these two chemical formulas. Unfortunately, coelution did  
 467 not fully allow exploiting MS/MS fragmentation carried out on the two chemical formulas, and to formally identify  
 468 the two compounds. There is still a lot of characterization work to be done, but the hypothesis of common isomeric  
 469 products formed through an autoxidation mechanism operating in atmospheric and low-temperature combustion  
 470 conditions seems to be confirmed.

471 **Table 4.** Isomers of  $\alpha$ -pinene and limonene oxidation reported in the literature.

	$C_{10}H_{16}O_2$		$C_{10}H_{16}O_3$	
$\alpha$ -pinene	Pinonaldehyde	(Fang et al., 2017)	Pinonic acid	(Fang et al., 2017;Ng et al., 2011;Meusinger et al., 2017)
	hydroxyketone	(Fang et al., 2017)	hydroxy pinonaldehydes	(Fang et al., 2017;Meusinger et al., 2017)
Limonene	limononaldehyde	(Fang et al., 2017;Walser et al., 2008;Bateman et al., 2009)	limononic acid	(Fang et al., 2017;Witkowski and Gierczak, 2017;Hammes et al., 2019;Walser et al., 2008;Bateman et al., 2009;Warscheid and Hoffmann, 2001)
	4-isopropenyl-methylhydroxy-2-oxocyclohexane	(Fang et al., 2017)	7-hydroxy-limononaldehyde	(Fang et al., 2017;Walser et al., 2008;Bateman et al., 2009;Meusinger et al., 2017)

472

## 473 5 Conclusion

474 The oxidation of limonene-oxygen-nitrogen and  $\alpha$ -pinene-oxygen-nitrogen mixtures was carried out using a jet-  
 475 stirred reactor at elevated temperature (590 K), a residence time of 2 s, and atmospheric pressure. The products  
 476 were analyzed by liquid chromatography, flow injection, and soft ionization-high resolution mass spectrometry.  
 477 H/D exchange and 2,4-dinitrophenyl hydrazine derivatization were used to assess the presence of OOH and C=O  
 478 groups in products, respectively. We probed the effects of the type of ionization used in mass spectrometry analyses  
 479 on the detection of oxidation products. Heated electrospray ionization (HESI +/-) and atmospheric pressure  
 480 chemical ionization (APCI +/-) were used. A large dataset was obtained and compared with literature data obtained  
 481 during the oxidation of limonene and  $\alpha$ -pinene under simulated tropospheric and low-temperature oxidation  
 482 conditions. This work showed a surprisingly similar set of chemical formulas of products, including oligomers,  
 483 formed under the two rather different conditions, i.e., cool flames and simulated atmospheric oxidation. Data  
 484 analysis involving van Krevelen diagrams, oxygen number distribution, oxidation state of carbon, and chemical  
 485 relationship between molecules, indicated that a subset of chemical formulas is common to all experiments  
 486 independently of experimental conditions. More than 35% of the chemical formulas detected in combustion  
 487 chemistry experiments using a JSR have been detected in the studies carried out under atmospheric conditions.

488 Finally, we have outlined the existence of a substantial common dataset of autoxidation products. This result tends  
489 to show that autoxidation is indeed inducing similarity between atmospheric and combustion products. Detailed  
490 analysis of our data was performed by UHPLC-MS/MS of selected chemical formulas observed in the literature.  
491 Nevertheless, final identification was not possible due to coelutions.

492 The present JSR data could be useful to atmospheric chemists working in the field of wildfire and/or biomass  
493 burning induced air pollution. Considering that low-temperature oxidation (cool flame) products, i.e., VOCs, can  
494 be emitted from biomass burning, wildfires and engine exhausts, the present data should be of interest for the  
495 atmospheric chemists because they complement those obtained in atmospheric chemistry literature. It would be  
496 interesting to complement the atmospheric relevant data with MS<sup>2</sup> analyses of products and assessment of the  
497 presence of hydroperoxyl and carbonyl groups HOMs. Further MS<sup>2</sup> characterizations are also needed for the  
498 products observed in the present work. Finally, a study of the temperature dependence of products formation would  
499 be very useful, both under cool flame conditions and simulated atmospheric oxidation conditions.

500

## 501 **Acknowledgements**

502 The authors gratefully acknowledge funding from the Labex Caprysses (ANR-11-LABX-0006-01), the Labex  
503 Voltaire (ANR-10-LABX-100-01), CPER, and EFRD (PROMESTOCK and APPROPOR-e projects) and the  
504 French MESRI for a Ph.D. grant. We also thank (Tomaz et al., 2021) for sharing experimental data on limonene  
505 oxidation.

506

## 507 **References**

- 508 Bailey, H. C., and Norrish, R. G. W.: The oxidation of hexane in the cool-flame region, Proceedings of  
509 the Royal Society of London Series a-Mathematical and Physical Sciences, 212, 311-330,  
510 <https://doi.org/10.1098/rspa.1952.0084>, 1952.
- 511 Bateman, A. P., Nizkorodov, S. A., Laskin, J., and Laskin, A.: Time-resolved molecular characterization  
512 of limonene/ozone aerosol using high-resolution electrospray ionization mass spectrometry,  
513 Physical Chemistry Chemical Physics, 11, 7931-7942, <https://doi.org/10.1039/B905288G>, 2009.
- 514 Belhadj, N., Benoit, R., Dagaut, P., Lailliau, M., Serinyel, Z., Dayma, G., Khaled, F., Moreau, B., and  
515 Foucher, F.: Oxidation of di-n-butyl ether: Experimental characterization of low-temperature  
516 products in JSR and RCM, Combustion and Flame, 222, 133-144,  
517 <https://doi.org/10.1016/j.combustflame.2020.08.037>, 2020.
- 518 Belhadj, N., Benoit, R., Dagaut, P., and Lailliau, M.: Experimental characterization of n-heptane low-  
519 temperature oxidation products including keto-hydroperoxides and highly oxygenated organic  
520 molecules (HOMs), Combustion and Flame, 224, 83-93,  
521 <https://doi.org/10.1016/j.combustflame.2020.10.021>, 2021a.
- 522 Belhadj, N., Lailliau, M., Benoit, R., and Dagaut, P.: Towards a Comprehensive Characterization of the  
523 Low-Temperature Autoxidation of Di-n-Butyl Ether, Molecules, 26, 7174, 2021b.
- 524 Belhadj, N., Lailliau, M., Benoit, R., and Dagaut, P.: Experimental and kinetic modeling study of n-  
525 hexane oxidation. Detection of complex low-temperature products using high-resolution mass  
526 spectrometry, Combustion and Flame, 233, 111581,  
527 <https://doi.org/10.1016/j.combustflame.2021.111581>, 2021c.
- 528 Benoit, R., Belhadj, N., Lailliau, M., and Dagaut, P.: On the similarities and differences between the  
529 products of oxidation of hydrocarbons under simulated atmospheric conditions and cool flames,  
530 Atmos. Chem. Phys., 21, 7845-7862, <https://doi.org/10.5194/acp-21-7845-2021>, 2021.

- 531 Benson, S. W.: The kinetics and thermochemistry of chemical oxidation with application to  
532 combustion and flames, *Progress in Energy and Combustion Science*, 7, 125-134,  
533 [https://doi.org/10.1016/0360-1285\(81\)90007-1](https://doi.org/10.1016/0360-1285(81)90007-1), 1981.
- 534 Bernath, P., Boone, C., and Crouse, J.: Wildfire smoke destroys stratospheric ozone, *Science*, 375,  
535 1292-1295, <https://doi.org/10.1126/science.abm5611>, 2022.
- 536 Berndt, T., Richters, S., Kaethner, R., Voigtländer, J., Stratmann, F., Sipilä, M., Kulmala, M., and  
537 Herrmann, H.: Gas-Phase Ozonolysis of Cycloalkenes: Formation of Highly Oxidized RO<sub>2</sub> Radicals  
538 and Their Reactions with NO, NO<sub>2</sub>, SO<sub>2</sub>, and Other RO<sub>2</sub> Radicals, *The Journal of Physical  
539 Chemistry A*, 119, 10336-10348, <https://doi.org/10.1021/acs.jpca.5b07295>, 2015.
- 540 Berndt, T., Richters, S., Jokinen, T., Hyttinen, N., Kurtén, T., Otkjær, R. V., Kjaergaard, H. G.,  
541 Stratmann, F., Herrmann, H., Sipilä, M., Kulmala, M., and Ehn, M.: Hydroxyl radical-induced  
542 formation of highly oxidized organic compounds, *Nat Commun*, 7, 13677,  
543 <https://doi.org/10.1038/ncomms13677>, 2016.
- 544 Bianchi, F., Kurtén, T., Riva, M., Mohr, C., Rissanen, M. P., Roldin, P., Berndt, T., Crouse, J. D.,  
545 Wennberg, P. O., Mentel, T. F., Wildt, J., Junninen, H., Jokinen, T., Kulmala, M., Worsnop, D. R.,  
546 Thornton, J. A., Donahue, N., Kjaergaard, H. G., and Ehn, M.: Highly Oxygenated Organic  
547 Molecules (HOM) from Gas-Phase Autoxidation Involving Peroxy Radicals: A Key Contributor to  
548 Atmospheric Aerosol, *Chemical Reviews*, 119, 3472-3509,  
549 <https://doi.org/10.1021/acs.chemrev.8b00395>, 2019.
- 550 Burke, M., Driscoll, A., Heft-Neal, S., Xue, J., Burney, J., and Wara, M.: The changing risk and burden  
551 of wildfire in the United States, *Proceedings of the National Academy of Sciences*, 118,  
552 e2011048118, doi:10.1073/pnas.2011048118, 2021.
- 553 Camredon, M., Hamilton, J. F., Alam, M. S., Wyche, K. P., Carr, T., White, I. R., Monks, P. S., Rickard, A.  
554 R., and Bloss, W. J.: Distribution of gaseous and particulate organic composition during dark  
555  $\alpha$ -pinene ozonolysis, *Atmos. Chem. Phys.*, <https://doi.org/10.2893-2917>,  
556 <https://doi.org/10.5194/acp-10-2893-2010>, 2010.
- 557 Cox, R. A., and Cole, J. A.: Chemical aspects of the autoignition of hydrocarbon-air mixtures, *Combust.  
558 Flame*, 60, 109-123, [https://doi.org/10.1016/0010-2180\(85\)90001-X](https://doi.org/10.1016/0010-2180(85)90001-X), 1985.
- 559 Crouse, J. D., Nielsen, L. B., Jørgensen, S., Kjaergaard, H. G., and Wennberg, P. O.: Autoxidation of  
560 organic compounds in the atmosphere, *J. Phys. Chem. Lett.*, 4, 3513, 2013.
- 561 Dagaut, P., Cathonnet, M., Rouan, J. P., Foulatier, R., Quilgars, A., Boettner, J. C., Gaillard, F., and  
562 James, H.: A jet-stirred reactor for kinetic studies of homogeneous gas-phase reactions at  
563 pressures up to ten atmospheres ( $\approx 1$  MPa), *Journal of Physics E: Scientific Instruments*, 19, 207-  
564 209, <https://doi.org/10.1088/0022-3735/19/3/009>, 1986.
- 565 Dagaut, P., Cathonnet, M., Boettner, J. C., and Gaillard, F.: Kinetic Modeling of Propane Oxidation,  
566 *Combustion Science and Technology*, 56, 23-63, <https://doi.org/10.1080/00102208708947080>,  
567 1987.
- 568 Dagaut, P., Cathonnet, M., Boettner, J. C., and Gaillard, F.: Kinetic modeling of ethylene oxidation,  
569 *Combustion and Flame*, 71, 295-312, [https://doi.org/10.1016/0010-2180\(88\)90065-X](https://doi.org/10.1016/0010-2180(88)90065-X), 1988.
- 570 Deng, Y., Inomata, S., Sato, K., Ramasamy, S., Morino, Y., Enami, S., and Tanimoto, H.: Temperature  
571 and acidity dependence of secondary organic aerosol formation from  $\alpha$ -pinene ozonolysis with a  
572 compact chamber system, *Atmos. Chem. Phys.*, 21, 5983-6003, <https://doi.org/10.5194/acp-21-5983-2021>, 2021.
- 574 Ehn, M., Thornton, J. A., Kleist, E., Sipilä, M., Junninen, H., Pullinen, I., Springer, M., Rubach, F.,  
575 Tillmann, R., Lee, B., Lopez-Hilfiker, F., Andres, S., Acir, I. H., Rissanen, M., Jokinen, T.,  
576 Schobesberger, S., Kangasluoma, J., Kontkanen, J., Nieminen, T., Kurten, T., Nielsen, L. B.,  
577 Jørgensen, S., Kjaergaard, H. G., Canagaratna, M., Maso, M. D., Berndt, T., Petaja, T., Wahner, A.,  
578 Kerminen, V. M., Kulmala, M., Worsnop, D. R., Wildt, J., and Mentel, T. F.: A large source of low-  
579 volatility secondary organic aerosol, *Nature*, 506, 476-479, <https://doi.org/10.1038/nature13032>,  
580 2014.
- 581 Fang, W., Gong, L., and Sheng, L.: Online analysis of secondary organic aerosols from OH-initiated  
582 photooxidation and ozonolysis of  $\alpha$ -pinene,  $\beta$ -pinene,  $\Delta^3$ -carene and d-limonene by thermal

- 583 desorption–photoionisation aerosol mass spectrometry, *Environmental Chemistry*, 14, 75-90,  
584 <https://doi.org/10.1071/EN16128>, 2017.
- 585 Gilman, J. B., Lerner, B. M., Kuster, W. C., Goldan, P. D., Warneke, C., Veres, P. R., Roberts, J. M., de  
586 Gouw, J. A., Burling, I. R., and Yokelson, R. J.: Biomass burning emissions and potential air quality  
587 impacts of volatile organic compounds and other trace gases from fuels common in the US,  
588 *Atmos. Chem. Phys.*, 15, 13915-13938, <https://doi.org/10.5194/acp-15-13915-2015>, 2015.
- 589 Hammes, J., Lutz, A., Mentel, T., Faxon, C., and Hallquist, M.: Carboxylic acids from limonene  
590 oxidation by ozone and hydroxyl radicals: insights into mechanisms derived using a FIGAERO-  
591 CIMS, *Atmos. Chem. Phys.*, 19, 13037-13052, <https://doi.org/10.5194/acp-19-13037-2019>, 2019.
- 592 Harvey, B. G., Wright, M. E., and Quintana, R. L.: High-Density Renewable Fuels Based on the  
593 Selective Dimerization of Pinenes, *Energy Fuels*, 24, 267-273, <https://doi.org/10.1021/ef900799c>,  
594 2010.
- 595 Harvey, B. G., Merriman, W. W., and Koontz, T. A.: High-Density Renewable Diesel and Jet Fuels  
596 Prepared from Multicyclic Sesquiterpanes and a 1-Hexene-Derived Synthetic Paraffinic Kerosene,  
597 *Energy Fuels*, 29, 2431-2436, <https://doi.org/10.1021/ef5027746>, 2015.
- 598 Hatch, L. E., Jen, C. N., Kreisberg, N. M., Selimovic, V., Yokelson, R. J., Stamatidis, C., York, R. A., Foster,  
599 D., Stephens, S. L., Goldstein, A. H., and Barsanti, K. C.: Highly Speciated Measurements of  
600 Terpenoids Emitted from Laboratory and Mixed-Conifer Forest Prescribed Fires, *Environmental*  
601 *Science & Technology*, 53, 9418-9428, <https://doi.org/10.1021/acs.est.9b02612>, 2019.
- 602 Hecht, E. S., Scigelova, M., Eliuk, S., and Makarov, A.: Fundamentals and Advances of Orbitrap Mass  
603 Spectrometry, *Encyclopedia of Analytical Chemistry*, 1-40,  
604 <https://doi.org/10.1002/9780470027318.a9309.pub2>, 2019.
- 605 Hu, Y., Fernandez-Anez, N., Smith, T. E. L., and Rein, G.: Review of emissions from smouldering peat  
606 fires and their contribution to regional haze episodes, *International Journal of Wildland Fire*, 27,  
607 293-312, <https://doi.org/10.1071/WF17084>, 2018.
- 608 Huang, W., Saathoff, H., Pajunoja, A., Shen, X., Naumann, K. H., Wagner, R., Virtanen, A., Leisner, T.,  
609 and Mohr, C.:  $\alpha$ -Pinene secondary organic aerosol at low temperature: chemical composition and  
610 implications for particle viscosity, *Atmos. Chem. Phys.*, 18, 2883-2898,  
611 <https://doi.org/10.5194/acp-18-2883-2018>, 2018.
- 612 Iyer, S., Rissanen, M. P., Valiev, R., Barua, S., Krechmer, J. E., Thornton, J., Ehn, M., and Kurtén, T.:  
613 Molecular mechanism for rapid autoxidation in  $\alpha$ -pinene ozonolysis, *Nature Communications*, 12,  
614 878, <https://doi.org/10.1038/s41467-021-21172-w>, 2021.
- 615 Jokinen, T., Sipilä, M., Richters, S., Kerminen, V.-M., Paasonen, P., Stratmann, F., Worsnop, D.,  
616 Kulmala, M., Ehn, M., Herrmann, H., and Berndt, T.: Rapid Autoxidation Forms Highly Oxidized  
617 RO<sub>2</sub> Radicals in the Atmosphere, *Angewandte Chemie International Edition*, 53, 14596-14600,  
618 <https://doi.org/10.1002/anie.201408566>, 2014a.
- 619 Jokinen, T., Sipilä, M., Richters, S., Kerminen, V. M., Paasonen, P., Stratmann, F., Worsnop, D.,  
620 Kulmala, M., Ehn, M., and Herrmann, H.: Rapid autoxidation forms highly oxidized RO<sub>2</sub> radicals in  
621 the atmosphere, *Angew. Chem., Int. Ed.*, 53, 14596, 2014b.
- 622 Jokinen, T., Berndt, T., Makkonen, R., Kerminen, V.-M., Junninen, H., Paasonen, P., Stratmann, F.,  
623 Herrmann, H., Guenther, A. B., Worsnop, D. R., Kulmala, M., Ehn, M., and Sipilä, M.: Production of  
624 extremely low volatile organic compounds from biogenic emissions: Measured yields and  
625 atmospheric implications, *Proceedings of the National Academy of Sciences*, 112, 7123-7128,  
626 <https://doi.org/10.1073/pnas.1423977112>, 2015.
- 627 Kekäläinen, T., Pakarinen, J. M. H., Wickström, K., Lobodin, V. V., McKenna, A. M., and Jänis, J.:  
628 Compositional Analysis of Oil Residues by Ultrahigh-Resolution Fourier Transform Ion Cyclotron  
629 Resonance Mass Spectrometry, *Energy Fuels*, 27, 2002-2009, <https://doi.org/10.1021/ef301762v>,  
630 2013.
- 631 Khaykin, S., Legras, B., Bucci, S., Sellitto, P., Isaksen, I., Tencé, F., Bekki, S., Bourassa, A., Rieger, L.,  
632 Zawada, D., Jumelet, J., and Godin-Beekmann, S.: The 2019/20 Australian wildfires generated a  
633 persistent smoke-charged vortex rising up to 35 km altitude, *Communications Earth &*  
634 *Environment*, 1, 22, <https://doi.org/10.1038/s43247-020-00022-5>, 2020.

- 635 Kobziar, L. N., Pingree, M. R. A., Larson, H., Dreaden, T. J., Green, S., and Smith, J. A.:  
636 Pyroaerobiology: the aerosolization and transport of viable microbial life by wildland fire,  
637 *Ecosphere*, 9, e02507, <https://doi.org/10.1002/ecs2.2507>, 2018.
- 638 Korcek, S., Ingold, K. U., Chenier, J. H. B., and Howard, J. A.: Absolute rate constants for hydrocarbon  
639 autoxidation .21. Activation-energies for propagation and correlation of propagation rate  
640 constants with carbon-hydrogen bond strengths, *Canadian Journal of Chemistry*, 50, 2285-&  
641 <https://doi.org/10.1139/v72-365>, 1972.
- 642 Kourtchev, I., Doussin, J. F., Giorio, C., Mahon, B., Wilson, E. M., Maurin, N., Pangui, E., Venables, D.  
643 S., Wenger, J. C., and Kalberer, M.: Molecular Composition of Fresh and Aged Secondary Organic  
644 Aerosol from a Mixture of Biogenic Volatile Compounds: A High-Resolution Mass Spectrometry  
645 Study, *Atmos. Chem. Phys.*, 15, 5683, 2015.
- 646 Krechmer, J. E., Groessl, M., Zhang, X., Junninen, H., Massoli, P., Lambe, A. T., Kimmel, J. R., Cubison,  
647 M. J., Graf, S., Lin, Y. H., Budisulistiorini, S. H., Zhang, H., Surratt, J. D., Knochenmuss, R., Jayne, J.  
648 T., Worsnop, D. R., Jimenez, J. L., and Canagaratna, M. R.: Ion mobility spectrometry–mass  
649 spectrometry (IMS–MS) for on- and offline analysis of atmospheric gas and aerosol species,  
650 *Atmos. Meas. Tech.*, 9, 3245-3262, <https://doi.org/10.5194/amt-9-3245-2016>, 2016.
- 651 Kristensen, K., Watne, Å. K., Hammes, J., Lutz, A., Petäjä, T., Hallquist, M., Bilde, M., and Glasius, M.:  
652 High-Molecular Weight Dimer Esters Are Major Products in Aerosols from  $\alpha$ -Pinene Ozonolysis  
653 and the Boreal Forest, *Environmental Science & Technology Letters*, 3, 280-285,  
654 <https://doi.org/10.1021/acs.estlett.6b00152>, 2016.
- 655 Kroll, J. H., Donahue, N. M., Jimenez, J. L., Kessler, S. H., Canagaratna, M. R., Wilson, K. R., Altieri, K.  
656 E., Mazzoleni, L. R., Wozniak, A. S., Bluhm, H., Mysak, E. R., Smith, J. D., Kolb, C. E., and Worsnop,  
657 D. R.: Carbon oxidation state as a metric for describing the chemistry of atmospheric organic  
658 aerosol, *Nature Chemistry*, 3, 133-139, <https://doi.org/10.1038/nchem.948>, 2011.
- 659 Kundu, S., Fisseha, R., Putman, A. L., Rahn, T. A., and Mazzoleni, L. R.: High molecular weight SOA  
660 formation during limonene ozonolysis: insights from ultrahigh-resolution FT-ICR mass  
661 spectrometry characterization, *Atmos. Chem. Phys.*, 12, 5523-5536, [https://doi.org/10.5194/acp-](https://doi.org/10.5194/acp-12-5523-2012)  
662 [12-5523-2012](https://doi.org/10.5194/acp-12-5523-2012), 2012.
- 663 Kurtén, T., Rissanen, M. P., Mackeprang, K., Thornton, J. A., Hyttinen, N., Jørgensen, S., Ehn, M., and  
664 Kjaergaard, H. G.: Computational Study of Hydrogen Shifts and Ring-Opening Mechanisms in  $\alpha$ -  
665 Pinene Ozonolysis Products, *The Journal of Physical Chemistry A*, 119, 11366-11375,  
666 <https://doi.org/10.1021/acs.jpca.5b08948>, 2015.
- 667 Melendez-Perez, J. J., Martínez-Mejía, M. J., and Eberlin, M. N.: A reformulated aromaticity index  
668 equation under consideration for non-aromatic and non-condensed aromatic cyclic carbonyl  
669 compounds, *Organic Geochemistry*, 95, 29-33,  
670 <https://doi.org/10.1016/j.orggeochem.2016.02.002>, 2016.
- 671 Meusinger, C., Dusek, U., King, S. M., Holzinger, R., Rosenørn, T., Sperlich, P., Julien, M., Remaud, G.  
672 S., Bilde, M., Röckmann, T., and Johnson, M. S.: Chemical and isotopic composition of secondary  
673 organic aerosol generated by  $\alpha$ -pinene ozonolysis, *Atmos. Chem. Phys.*, 17, 6373-6391,  
674 <https://doi.org/10.5194/acp-17-6373-2017>, 2017.
- 675 Mewalal, R., Rai, D. K., Kainer, D., Chen, F., Külheim, C., Peter, G. F., and Tuskan, G. A.: Plant-Derived  
676 Terpenes: A Feedstock for Specialty Biofuels, *Trends Biotechnol.*, 35, 227-240,  
677 <https://doi.org/10.1016/j.tibtech.2016.08.003>, 2017.
- 678 Ng, N. L., Canagaratna, M. R., Jimenez, J. L., Chhabra, P. S., Seinfeld, J. H., and Worsnop, D. R.:  
679 Changes in organic aerosol composition with aging inferred from aerosol mass spectra, *Atmos.*  
680 *Chem. Phys.*, 11, 6465-6474, <https://doi.org/10.5194/acp-11-6465-2011>, 2011.
- 681 Nørgaard, A. W., Vibenholt, A., Benassi, M., Clausen, P. A., and Wolkoff, P.: Study of Ozone-Initiated  
682 Limonene Reaction Products by Low Temperature Plasma Ionization Mass Spectrometry, *Journal*  
683 *of The American Society for Mass Spectrometry*, 24, <https://doi.org/1090-1096>, 10.1007/s13361-  
684 013-0648-3, 2013.
- 685 Nozière, B., Kalberer, M., Claeys, M., Allan, J., D'Anna, B., Decesari, S., Finessi, E., Glasius, M., Grgić, I.,  
686 Hamilton, J. F., Hoffmann, T., Iinuma, Y., Jaoui, M., Kahnt, A., Kampf, C. J., Kourtchev, I.,

- 687 Maenhaut, W., Marsden, N., Saarikoski, S., Schnelle-Kreis, J., Surratt, J. D., Szidat, S., Szmigielski,  
688 R., and Wisthaler, A.: The Molecular Identification of Organic Compounds in the Atmosphere:  
689 State of the Art and Challenges, *Chemical Reviews*, 115, 3919-3983,  
690 <https://doi.org/10.1021/cr5003485>, 2015.
- 691 Otkjær, R. V., Jakobsen, H. H., Tram, C. M., and Kjaergaard, H. G.: Calculated Hydrogen Shift Rate  
692 Constants in Substituted Alkyl Peroxy Radicals, *The Journal of Physical Chemistry A*, 122, 8665-  
693 8673, <https://doi.org/10.1021/acs.jpca.8b06223>, 2018.
- 694 Popovicheva, O. B., Engling, G., Ku, I. T., Timofeev, M. A., and Shonija, N. K.: Aerosol Emissions from  
695 Long-lasting Smoldering of Boreal Peatlands: Chemical Composition, Markers, and Microstructure,  
696 *Aerosol and Air Quality Research*, 19, 484-503, <https://doi.org/10.4209/aaqr.2018.08.0302>, 2019.
- 697 Prichard, S. J., O'Neill, S. M., Eagle, P., Andreu, A. G., Drye, B., Dubowy, J., Urbanski, S., and Strand, T.  
698 M.: Wildland fire emission factors in North America: synthesis of existing data, measurement  
699 needs and management applications, *International Journal of Wildland Fire*, 29, 132-147,  
700 <https://doi.org/10.1071/WF19066>, 2020.
- 701 Quéléver, L. L. J., Kristensen, K., Normann Jensen, L., Rosati, B., Teiwes, R., Daellenbach, K. R.,  
702 Peräkylä, O., Roldin, P., Bossi, R., Pedersen, H. B., Glasius, M., Bilde, M., and Ehn, M.: Effect of  
703 temperature on the formation of highly oxygenated organic molecules (HOMs) from alpha-pinene  
704 ozonolysis, *Atmos. Chem. Phys.*, 19, 7609-7625, <https://doi.org/10.5194/acp-19-7609-2019>, 2019.
- 705 Riva, M., Rantala, P., Krechmer, J. E., Peräkylä, O., Zhang, Y., Heikkinen, L., Garmash, O., Yan, C.,  
706 Kulmala, M., Worsnop, D., and Ehn, M.: Evaluating the performance of five different chemical  
707 ionization techniques for detecting gaseous oxygenated organic species, *Atmos. Meas. Tech.*, 12,  
708 2403-2421, <https://doi.org/10.5194/amt-12-2403-2019>, 2019.
- 709 Savee, J. D., Papajak, E., Rotavera, B., Huang, H., Eskola, A. J., Welz, O., Sheps, L., Taatjes, C. A., Zádor,  
710 J., and Osborn, D. L.: Carbon radicals. Direct observation and kinetics of a hydroperoxyalkyl radical  
711 (QOOH), *Science*, 347, 643-646, <https://doi.org/10.1126/science.aaa1495>, 2015.
- 712 Schneider, E., Czech, H., Popovicheva, O., Lütke, H., Schnelle-Kreis, J., Khodzher, T., Rüger, C. P., and  
713 Zimmermann, R.: Molecular Characterization of Water-Soluble Aerosol Particle Extracts by  
714 Ultrahigh-Resolution Mass Spectrometry: Observation of Industrial Emissions and an  
715 Atmospherically Aged Wildfire Plume at Lake Baikal, *ACS Earth and Space Chemistry*, 6, 1095-  
716 1107, <https://doi.org/10.1021/acsearthspacechem.2c00017>, 2022.
- 717 Seinfeld, J. H., and Pandis, S. N.: *Atmospheric Chemistry and Physics: From Air Pollution to Climate*  
718 *Change*, 2nd ed., Wiley-Interscience, Hoboken, NJ, 1232 pp., 2006.
- 719 Smith, J. S., Laskin, A., and Laskin, J.: Molecular Characterization of Biomass Burning Aerosols Using  
720 High-Resolution Mass Spectrometry, *Analytical Chemistry*, 81, 1512-1521,  
721 <https://doi.org/10.1021/ac8020664>, 2009.
- 722 Tomaz, S., Wang, D., Zabalegui, N., Li, D., Lamkaddam, H., Bachmeier, F., Vogel, A., Monge, M. E.,  
723 Perrier, S., Baltensperger, U., George, C., Rissanen, M., Ehn, M., El Haddad, I., and Riva, M.:  
724 Structures and reactivity of peroxy radicals and dimeric products revealed by online tandem mass  
725 spectrometry, *Nature Communications*, 12, 300, <https://doi.org/10.1038/s41467-020-20532-2>,  
726 2021.
- 727 Tröstl, J., Chuang, W. K., Gordon, H., Heinritzi, M., Yan, C., Molteni, U., Ahlm, L., Frege, C., Bianchi, F.,  
728 Wagner, R., Simon, M., Lehtipalo, K., Williamson, C., Craven, J. S., Duplissy, J., Adamov, A.,  
729 Almeida, J., Bernhammer, A.-K., Breitenlechner, M., Brilke, S., Dias, A., Ehrhart, S., Flagan, R. C.,  
730 Franchin, A., Fuchs, C., Guida, R., Gysel, M., Hansel, A., Hoyle, C. R., Jokinen, T., Junninen, H.,  
731 Kangasluoma, J., Keskinen, H., Kim, J., Krapf, M., Kürten, A., Laaksonen, A., Lawler, M., Leiminger,  
732 M., Mathot, S., Möhler, O., Nieminen, T., Onnela, A., Petäjä, T., Piel, F. M., Miettinen, P., Rissanen,  
733 M. P., Rondo, L., Sarnela, N., Schobesberger, S., Sengupta, K., Sipilä, M., Smith, J. N., Steiner, G.,  
734 Tomè, A., Virtanen, A., Wagner, A. C., Weingartner, E., Wimmer, D., Winkler, P. M., Ye, P., Carslaw,  
735 K. S., Curtius, J., Dommen, J., Kirkby, J., Kulmala, M., Riipinen, I., Worsnop, D. R., Donahue, N. M.,  
736 and Baltensperger, U.: The role of low-volatility organic compounds in initial particle growth in the  
737 atmosphere, *Nature*, 533, 527-531, <https://doi.org/10.1038/nature18271>, 2016.

- 738 Van Krevelen, D. W.: Graphical-statistical method for the study of structure and reaction processes of  
739 coal, *Fuel*, 29, 269-284, 1950.
- 740 Vereecken, L., Müller, J. F., and Peeters, J.: Low-volatility poly-oxygenates in the OH-initiated  
741 atmospheric oxidation of  $\alpha$ -pinene: impact of non-traditional peroxy radical chemistry, *Physical  
742 Chemistry Chemical Physics*, 9, 5241-5248, <https://doi.org/10.1039/B708023A>, 2007.
- 743 Walser, M. L., Desyaterik, Y., Laskin, J., Laskin, A., and Nizkorodov, S. A.: High-resolution mass  
744 spectrometric analysis of secondary organic aerosol produced by ozonation of limonene, *Physical  
745 Chemistry Chemical Physics*, 10, 1009-1022, <https://doi.org/10.1039/B712620D>, 2008.
- 746 Wang, Z., Popolan-Vaida, D. M., Chen, B., Moshhammer, K., Mohamed, S. Y., Wang, H., Sioud, S., Raji,  
747 M. A., Kohse-Höinghaus, K., Hansen, N., Dagaut, P., Leone, S. R., and Sarathy, S. M.: Unraveling the  
748 structure and chemical mechanisms of highly oxygenated intermediates in oxidation of organic  
749 compounds, *Proceedings of the National Academy of Sciences*, 114, 13102-13107,  
750 <https://doi.org/10.1073/pnas.1707564114>, 2017.
- 751 Wang, Z., Chen, B., Moshhammer, K., Popolan-Vaida, D. M., Sioud, S., Shankar, V. S. B., Vuilleumier, D.,  
752 Tao, T., Ruwe, L., Bräuer, E., Hansen, N., Dagaut, P., Kohse-Höinghaus, K., Raji, M. A., and Sarathy,  
753 S. M.: n-Heptane cool flame chemistry: Unraveling intermediate species measured in a stirred  
754 reactor and motored engine, *Combustion and Flame*, 187, 199-216,  
755 <https://doi.org/10.1016/j.combustflame.2017.09.003>, 2018.
- 756 Wang, Z., Ehn, M., Rissanen, M. P., Garmash, O., Quéléver, L., Xing, L., Monge Palacios, M., Rantala,  
757 P., Donahue, N. M., Berndt, T., and Sarathy, M.: - Efficient alkane oxidation under combustion  
758 engine and atmospheric conditions, *Communications Chemistry*, 4, 18,  
759 <https://doi.org/10.1038/s42004-020-00445-3>, 2021.
- 760 Warscheid, B., and Hoffmann, T.: Structural elucidation of monoterpene oxidation products by ion  
761 trap fragmentation using on-line atmospheric pressure chemical ionisation mass spectrometry in  
762 the negative ion mode, *Rapid Communications in Mass Spectrometry*, 15, 2259-2272,  
763 <https://doi.org/10.1002/rcm.504>, 2001.
- 764 Witkowski, B., and Gierczak, T.: Characterization of the limonene oxidation products with liquid  
765 chromatography coupled to the tandem mass spectrometry, *Atmospheric Environment*, 154, 297-  
766 307, <https://doi.org/10.1016/j.atmosenv.2017.02.005>, 2017.
- 767 Wotton, B. M., Gould, J. S., McCaw, W. L., Cheney, N. P., and Taylor, S. W.: Flame temperature and  
768 residence time of fires in dry eucalypt forest, *International Journal of Wildland Fire*, 21, 270-281,  
769 <https://doi.org/10.1071/WF10127>, 2012.
- 770 Xie, Q., Su, S., Chen, S., Xu, Y., Cao, D., Chen, J., Ren, L., Yue, S., Zhao, W., Sun, Y., Wang, Z., Tong, H.,  
771 Su, H., Cheng, Y., Kawamura, K., Jiang, G., Liu, C. Q., and Fu, P.: Molecular characterization of  
772 firework-related urban aerosols using Fourier transform ion cyclotron resonance mass  
773 spectrometry, *Atmos. Chem. Phys.*, 20, 6803-6820, <https://doi.org/10.5194/acp-20-6803-2020>,  
774 2020.
- 775 Zhang, H., Yee, L. D., Lee, B. H., Curtis, M. P., Worton, D. R., Isaacman-VanWertz, G., Offenberg, J. H.,  
776 Lewandowski, M., Kleindienst, T. E., Beaver, M. R., Holder, A. L., Lonneman, W. A., Docherty, K. S.,  
777 Jaoui, M., Pye, H. O. T., Hu, W., Day, D. A., Campuzano-Jost, P., Jimenez, J. L., Guo, H., Weber, R. J.,  
778 de Gouw, J., Koss, A. R., Edgerton, E. S., Brune, W., Mohr, C., Lopez-Hilfiker, F. D., Lutz, A.,  
779 Kreisberg, N. M., Spielman, S. R., Hering, S. V., Wilson, K. R., Thornton, J. A., and Goldstein, A. H.:  
780 Monoterpenes are the largest source of summertime organic aerosol in the southeastern United  
781 States, *Proceedings of the National Academy of Sciences*, 115, 2038-2043,  
782 <https://doi.org/10.1073/pnas.1717513115>, 2018.
- 783 Zhao, Y., Thornton, J. A., and Pye, H. O. T.: Quantitative constraints on autoxidation and dimer  
784 formation from direct probing of monoterpene-derived peroxy radical chemistry, *Proc Natl Acad  
785 Sci U S A*, 115, 12142-12147, <https://doi.org/10.1073/pnas.1812147115>, 2018.
- 786